

Final Report

ARTI Report No. 10090-02

ELECTRO-OSMOSIS FOR DEHUMIDIFICATION

Final Report

March 2008

Dr. David W. Gerlach



G. W. WOODRUFF SCHOOL OF MECHANICAL ENGINEERING
GEORGIA INSTITUTE OF TECHNOLOGY
801 Ferst Drive N.W.
Atlanta, Georgia 30332-0405

Prepared for

AIR-CONDITIONING AND REFRIGERATION TECHNOLOGY INSTITUTE, INC
4100 N. Fairfax Drive, Suite 200, Arlington, Virginia 22203-1678

DISCLAIMER

This report was prepared as an account of work sponsored by the Air-Conditioning and Refrigeration Technology Institute, Inc. (ARTI). Neither ARTI, its research program financial supporters, or any agency thereof, nor any of their employees, contractors, subcontractors or employees thereof - makes any warranty, expressed or implied; assumes any legal liability or responsibility for the accuracy, completeness, any third party's use of, or the results of such use of any information, apparatus, product, or process disclosed in this report; or represents that its use would not infringe privately owned rights. Reference herein to any specific commercial product, process, or service by trade name, trademark, manufacturer, or otherwise, does not necessarily constitute nor imply its endorsement, recommendation, or favoring by ARTI, its sponsors, or any agency thereof or their contractors or subcontractors. The views and opinions of authors expressed herein do not necessarily state or reflect those of ARTI, its program sponsors, or any agency thereof.

Funding for this project was provided by (listed alphabetically):

- Air-Conditioning & Refrigeration Institute (ARI)
- Copper Development Association (CDA)
- Heating, Refrigeration and Air Conditioning Institute of Canada (HRAI)
- New York State Energy Research and Development Authority (NYSERDA)

Final Report

TABLE OF CONTENTS

EXECUTIVE SUMMARY	iii
MAIN BODY OF REPORT	
BACKGROUND	1
PHASE 1 WORK.....	1
BASIS EXPLANATION OF ELECTROOSMOSIS	1
LITERATURE REVIEW UPDATE.....	2
INORGANIC MEMBRANE MODELING.....	2
FREE CONVECTION MEMBRANE EXPERIMENT	8
INORGANIC MEMBRANE EXPERIMENTS	11
NAFION® MEMBRANES	13
PROTON CONDUCTING POLYMER MEMBRANE MODEL.....	13
<i>Electroosmotic Flux Calculation</i>	13
<i>Model Results</i>	15
<i>Membrane Thickness</i>	15
NAFION® MEMBRANE EXPERIMENTS.....	17
<i>Comparison of Experiment to Model</i>	20
COMPARISON TO PRESENT TECHNOLOGY SYSTEM MODELING	20
<i>Process Air Conditions</i>	23
<i>Vapor Compression Cycle Efficiency</i>	23
COMPARISON TO PRESENT TECHNOLOGY SYSTEM RESULTS	23
<i>Membrane Surface Area</i>	24
<i>Adjustment for Experimental Results</i>	26
APPORTIONMENT OF SORPTION AND OHMIC HEAT	26
RECOMMENDATIONS FOR FUTURE WORK	30
CONCLUSIONS.....	30
REFERENCES	30

APPENDICES

APPENDIX A:	INORGANIC MEMBRANE MATERIAL PROPERTY TESTS	32
APPENDIX B:	FORCED CONVECTION MEMBRANE EXPERIMENT	34
APPENDIX C:	OTHER INORGANIC MATERIALS INVESTIGATED.....	35

LIST OF FIGURES

Figure 1:	Left: Schematic of pore, Right: H ⁺ ion.	2
Figure 2:	Schematic of electroosmotic dehumidification model.....	3
Figure 3:	Plot of water concentration in membrane	5
Figure 4:	Silica gel conductivity vs. water content	6
Figure 5:	Total flux through membrane	6
Figure 6:	Water concentration in membrane	7
Figure 7:	Electrical potential in membrane	7
Figure 8:	Electroosmotic flux as a function of position	8
Figure 9:	Schematic of free convection membrane experiment.....	9
Figure 10:	Dimension drawing of acrylic frame that holds the membrane.....	10
Figure 11:	Photos of silica gel concrete membrane.....	11
Figure 12:	Time series data of plaster membrane experiment	12
Figure 13:	Water flow in silica gel concrete membrane.....	13
Figure 14:	Water mass fluxes through membrane vs. thickness	16
Figure 15:	Total water mass flux through membrane vs. thickness.....	16
Figure 16:	Energy expended to pump of water vs. thickness.....	17
Figure 17:	Time series data of humidity ratios.....	18
Figure 18:	Electroosmotic and diffusion flows at 3 amp current	19
Figure 19:	Conventional and electroosmotic dehumidification systems.....	21
Figure 20:	Process paths of compared dehumidification systems.....	22
Figure 21:	Flow chart of technology comparison model.....	22
Figure 22:	COP as function of air mass flow rate	24
Figure 23:	Membrane area increases as voltage decreases	25
Figure 24:	COP increases with area	25
Figure 25:	Schematic of heat flows in membrane model	26
Figure 26:	Temperature of airstreams at constant ohmic heat flux	29
Figure 27:	Temperature of airstreams when the resistance varies with thickness	29
Figure A1:	Conductivity measurement techniques	33
Figure A2:	Streaming potential experiment design.....	34
Figure B1:	Schematic of forced convection membrane experiment.....	35
Figure C1:	Sodium silicate and silica gel membrane.....	36
Figure C2:	Loose silica gel membrane.....	36
Figure C3:	Agar- silica gel composite membrane.....	37

EXECUTIVE SUMMARY

Electro-osmosis for Dehumidification: Final Report

Electroosmosis has been proposed for dehumidification in air conditioning systems (Mina, 2003). This would allow the sensible and latent loads to be handled separately and may lead to improvements in energy efficiency and comfort control. In electroosmosis, water is pumped through channels or pores in solid material by the application of a voltage. A membrane composed of a desiccant material could remove moisture from air to be conditioned. Then, electroosmotic pumping could move the moisture across the membrane and reject it on the other side.

Earlier work on this project is recorded in the interim Phase 1 report (Gerlach, 2006). In Phase 1, literature pertinent to electroosmotic dehumidification was reviewed. A model was developed that computes the flow rate through the membrane as well as the water concentration and electrical potential profiles inside the membrane. In addition, experiments were proposed to test the validity of the model, prove the concept, and measure the membrane material properties. This report details further modeling, experiments completed, and a comparison of an electroosmotic dehumidification system to a current technology air conditioning system.

This report separately covers flow in inorganic media such as silica gel where there is bulk flow due to viscous drag and flow in organic ionomers where the flow is primarily the water in the solvation sheath of the mobile ions.

The model developed in Phase 1 for silica gel membranes has been transferred to Comsol (formerly Femlab), a finite element code allowing the modification and writing of the governing differential equations. This allows an increased number of elements in order to determine grid independence. The highly nonlinear relationship of relative humidity to silica gel electrical conductivity leads to highly nonlinear behavior in the model and instability.

A bench top experiment was developed to screen promising membrane materials and to provide data for model validation. Two sealed humidity chambers were separated by a membrane. The changes in the humidity were measured as current was applied to the membrane. A variety of membrane materials based on silica gel, Plaster of Paris, or zeolites were investigated. The most successful inorganic membrane was a silica gel concrete using Plaster of Paris as the cement and silica gel particles as the aggregate. The calculated total flux was 0.0015 mol/s-m^2 with an energy per mol of water pumped of 2 J/mol

Nafion[®], a sulfonated tetrafluoroethylene copolymer produced by DuPont, was tested in the same manner. Although, the electroosmotic flux was much higher than for the inorganic membranes, it was still three orders of magnitude smaller than that predicted. Further research is needed to reconcile the experimental data and modeling in order to determine feasibility.

The performance of an air conditioning system using an electroosmotic dehumidification system in series with a conventional vapor compression cycle was modeled. The electroosmotic system handles the entire latent load and the vapor compression system handles the entire sensible cooling load. Performance of the system was compared to a conventional vapor compression air conditioner that handles both the latent and sensible loads with a single evaporator coil. Modeling indicates the feasibility of electroosmotic dehumidification for separating the control of latent and sensible load in air conditioning systems. The total COP of the system, neglecting fan power, can be 1-2 times higher (depending on airflow rate) than a system using an evaporator for latent and sensible load.

Electro-Osmosis for Dehumidification Final Report

BACKGROUND

Electroosmosis has been proposed for dehumidification in air conditioning systems (Mina, 2003 and Gerlach, 2006). In electroosmosis, water is pumped through channels or pores in solid material by the application of a voltage. A membrane composed of a desiccant material removes moisture from air to be conditioned. Then, electroosmotic pumping moves the moisture across the membrane and rejects it on the other side. This allows the sensible and latent loads to be handled separately and may lead to improvements in energy efficiency and comfort control.

PHASE 1 WORK

Earlier work on this project is recorded in the interim Phase 1 report (Gerlach, 2006). In Phase 1, literature pertinent to electroosmotic dehumidification was reviewed. A model was developed that computes the flow rate through the membrane as well as the water concentration and electrical potential profiles inside the membrane. In addition, experiments were proposed to test the validity of the model, prove the concept, and measure the membrane material properties. This report details further modeling, experiments completed, and a comparison of an electroosmotic dehumidification system to a current technology air conditioning system.

BASIC EXPLANATION OF ELECTROOSMOSIS

Although water is a neutral molecule, it can be transported by the application of an electrical field. In a silica material such as a glass capillary or porous ceramic, the pore walls act as an acid, binding an OH^- , and donating H^+ ion to the water (Figure 1, left). The positive ion is typically considered to be a hydronium ion (H_3O^+), although other forms are predicted (Pivovar, 2005). Because the OH^- ions are bound to the wall, the H^+ ions are attracted to the wall to ensure overall electroneutrality. This forms a double layer of bound and free ions. The applied electric field causes the free ions to move. The electrical potential at a hypothetical slip plane between the free and bound ions is termed the zeta potential. The ions have a solvation shell of bound water molecules that moves with them (Figure 1: right). In the presence of bulk water, the movement of the solvated ions can move more water due to viscous forces. Because the moving

ions are close to the wall, the velocity gradient near the wall is very high. Away from the wall there is no net charge and therefore no net force from the electrical field. Consequently, the velocity profile far from the wall is flat. Similar principles apply in a wide variety of materials other than silica. This report separately covers flow in inorganic media such as silica gel where there is bulk flow due to viscous drag and flow in organic ionomers where the flow is primarily due to the water in the solvation sheath.

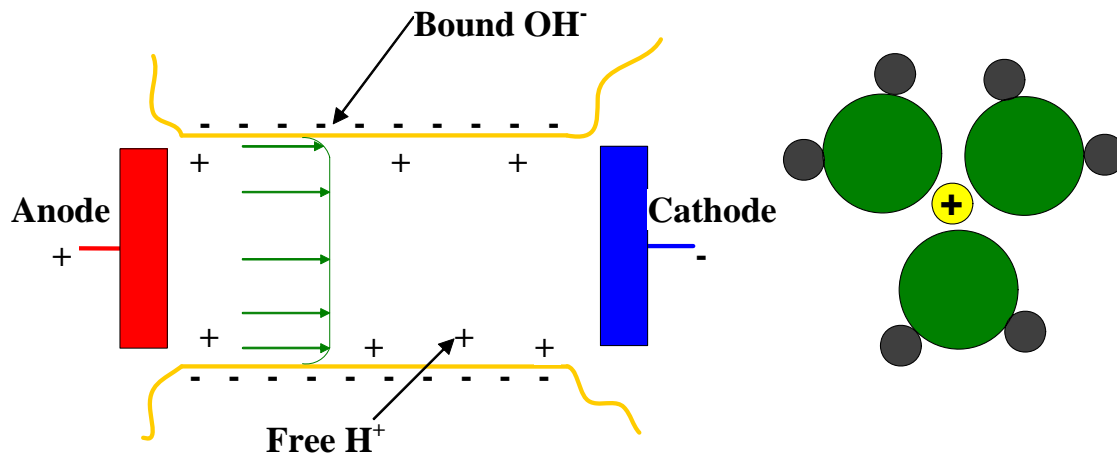


Figure 1: Left: Schematic of pore (Note: The numbers of positive and negative charges are equal in a real system.) Right: H⁺ ion surrounded by solvation shell of water molecules.

LITERATURE REVIEW UPDATE

A recent international patent (2007/099109) discloses the use of an electroosmotic membrane for dehumidification of air in a clothes dryer.

INORGANIC MEMBRANE MODELING

A model of silica gel membranes was developed in Phase 1. This model could also be extended to zeolite, plaster, or other inorganic materials. The model developed in Phase 1 was written in EES (Engineering Equation Solver) a Newton-Raphson solver highly dependent on initial guesses. In addition, the total number of variables allowed by the program limited the number of equations and elements.

The model has been transferred to Comsol (formerly Femlab), a finite element code allowing the modification and writing of the governing differential equations. This allows an increased number of elements in order to ensure grid independence.

The model calculates the total mass flux (\dot{m}''_{total}) as the sum of the forward flow of water by electroosmotic pumping (\dot{m}''_{bulk}) and the backward flow of water by diffusion ($\dot{m}''_{\text{diffusion}}$):

$$\dot{m}''_{\text{total}} = \dot{m}''_{\text{bulk}} + \dot{m}''_{\text{diffusion}}$$

At steady state the total mass flux is constant through each layer. However, the diffusive and electroosmotic fluxes vary with position (Figure 2). The moisture transport in the air was not modeled.

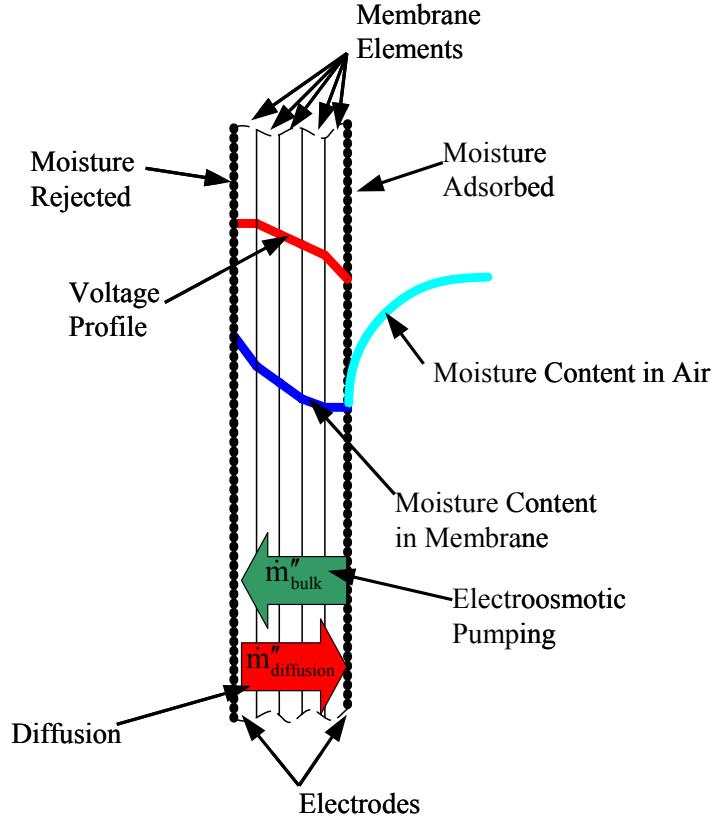


Figure 2: Schematic of electroosmotic dehumidification model

The electroosmotic mass flux (\dot{m}''_{bulk}) is dependent on the electrical potential gradient:

$$\dot{m}''_{\text{bulk}} = C_e \left(\frac{\rho_{\text{water}} \epsilon_{\text{water}} \zeta \Delta E_n}{\mu_{\text{water}} \Delta x} \right) \quad (1)$$

where ϵ_{water} is the electrical permittivity of water, ζ is the zeta potential of the surface (assumed to be 0.1 Volt), ρ_{water} is the water density, μ_{water} is the water viscosity, Δx is the membrane section thickness, and ΔE_n is the electrical potential difference across the membrane element.

The coefficient C_e is a function of the pore geometry, membrane porosity and tortuosity, and the

water content of the membrane. The important factors and functional form of C_e need to be determined by experiment. Appendix C of the Phase 1 report gives a description of the method used to calculate C_e . The value in the parentheses is the Helmholtz-Smoluchowski equation, which is the bulk velocity in a pore with a diameter much larger than the double layer thickness (Tikhomolova, 1993; Bard, 2001). This may need to be modified for very small pore sizes. The average electroosmotic coefficient, the ratio of flow to voltage gradient, was calculated by the EES code described in the Phase 1 project report.

The diffusion is generally proportional to the gradient of the water content (∇W):

$$\dot{m}_{\text{diffusion}}'' = -D\nabla W \quad (2)$$

The diffusion actually consists of the Fick's diffusion in the air and surface diffusion on the gel surface. In small pores, Knudsen diffusion may be dominating. These various effects are combined to get the overall diffusive flux. The effective diffusion constant D for each type of diffusion is dependent on the membrane porosity and tortuosity, and the water content of the membrane. The water content of the air can be calculated from the content of the membrane. Appendix C of the Phase 1 report gives a description of the method used to calculate the diffusion rate. The diffusion coefficient in the silica gel was also calculated as an average value by the EES model.

In order to ensure charge neutrality, the electrical current (i) through the membrane must be constant through each layer. The electrical conductivity of the silica gel in each element ($\text{Cond}_{\text{elec},n}$) varies with its water content (Anappara, 2004). Consequently, the electrical potential change across each element (ΔE_n) varies with position in the membrane:

$$R_{\text{elec},n} = \frac{\Delta x}{\text{Cond}_{\text{elec},n}} \quad (3)$$

$$\Delta E_n = iR_{\text{elec},n} \quad (4)$$

where $R_{\text{elec},n}$ is the electrical resistance of the element and i is the current density (amps/m²). In a real system the water concentration on the side being pumped from will be lower than that on the side being pumped to. As the membrane dries out the resistance to current flow increases, thus making the process self limiting. Therefore, the potential gradient across the membrane will not be constant.

The simulation results presented here are for a 1 cm thick silica gel membrane. The flow profile is assumed to be one-dimensional. The pressure on both sides of the membrane is assumed to be 1 atmosphere. The membrane is isothermal at 25°C. Concentration boundary conditions were used. On the high humidity side, the concentration at the surface was 12000 mol/m³ corresponding to a relative humidity of 67%. The side being pumped from had a concentration of 3000 mol/m³ corresponding to a relative humidity of 11%. The edges were at constant electrical potentials conditions of 0V and 10V.

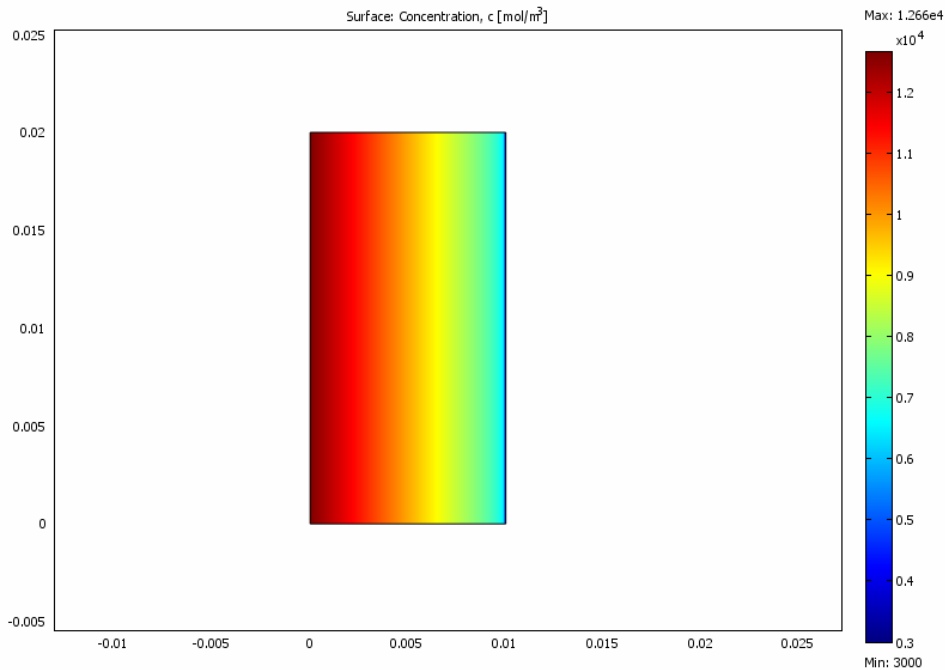


Figure 3: Plot of water concentration (mol/m³) in membrane. x and y axis labels are position in meters.

The concentration profile is shown in Figure 3 with electroosmotic flow from right to left. Figure 4 shows published data (Anappara, 2004) on the relationship between silica gel conductivity and water concentration. The conductance jumps four orders of magnitude over a relative humidity change of 58% to 81%. A highly nonlinear curve fit to this data was used in the COMSOL mode. This leads to highly nonlinear behavior in the model and instability (Figure 5). The stability of the answer is highly dependent on grid size. In the region of the membrane near the drier surface, where the water concentration changes (Figure 6), the conductivity changes dramatically. Consequently, the voltage gradient and the electroosmotic flux also

change dramatically (Figures 7 and 8). The grid size must be greatly reduced in this area to prevent instability.

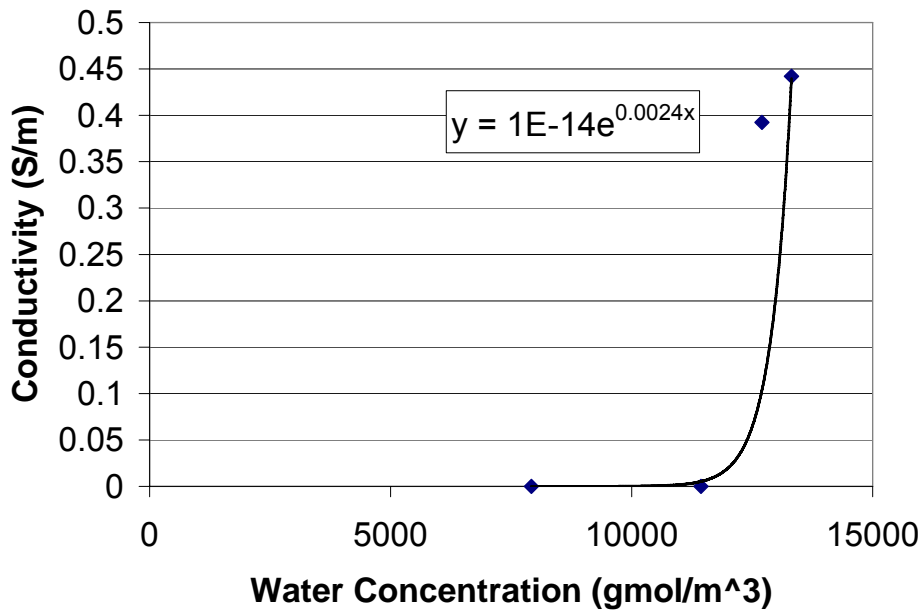


Figure 4: Published data on silica gel electrical conductivity vs. water content (Blue squares) and a curve fit to data (Anappara, 2004)

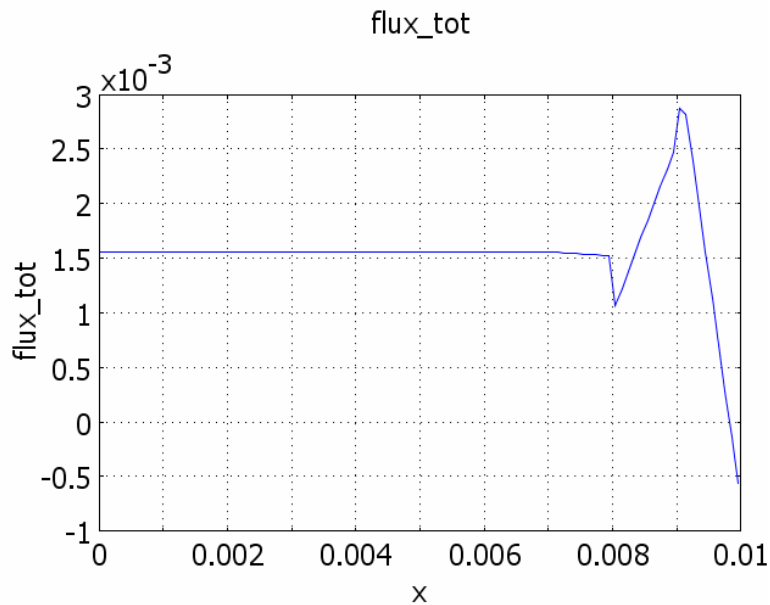


Figure 5: Graph of the total calculated flux (mol/m²-s) through the membrane showing instability due to nonlinearity. In this steady state model the flux should be constant through the whole membrane.

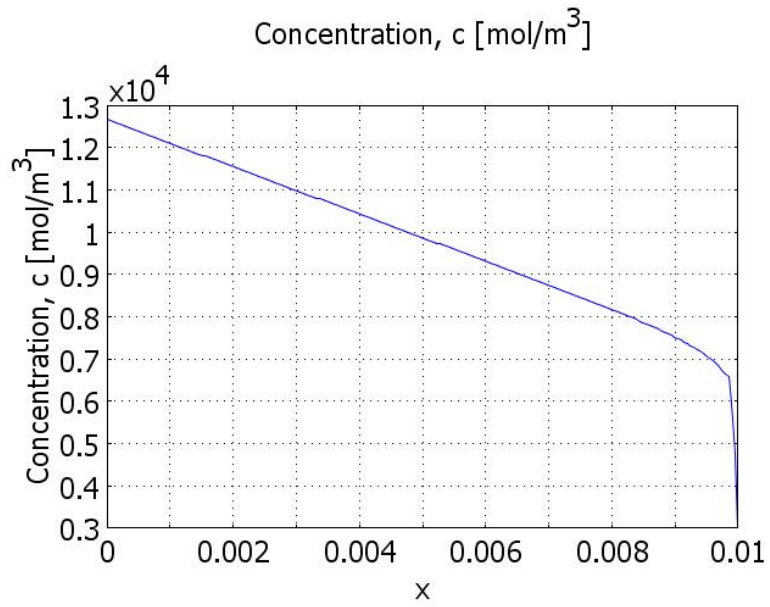


Figure 6: Water concentration in membrane as a function of position in meters through the membrane

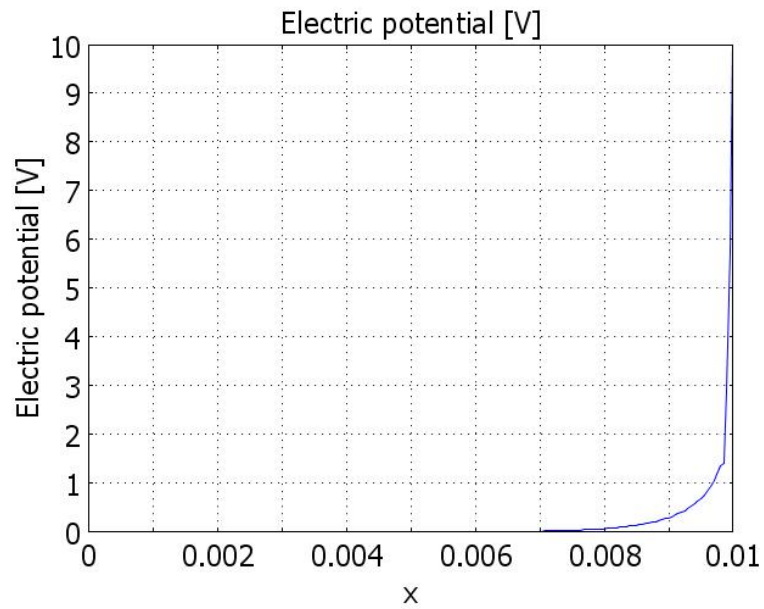


Figure 7: Electrical potential as a function of position in meters through the membrane

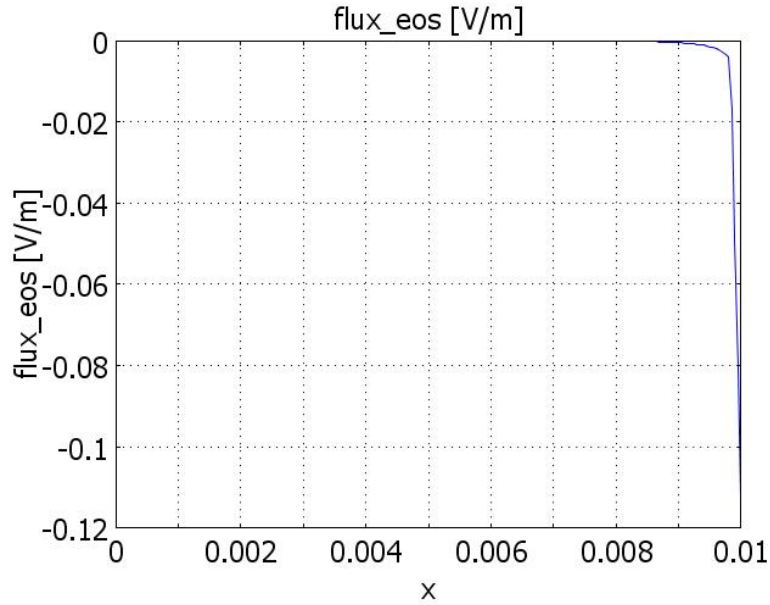


Figure 8: Electroosmotic flux ($\text{mol}/\text{m}^2\text{-s}$) as a function of position in meters through the membrane

The calculated total flux was $0.0015 \text{ mol}/\text{s}\text{-m}^2$ with a total power expended of $0.0031 \text{ W}/\text{m}^2$. This computes to an energy per mol of water pumped of $2 \text{ J}/\text{mol}$. This is only the energy needed to pump the water through the membrane and does not include the effects of the heats of adsorption and desorption.

FREE CONVECTION MEMBRANE EXPERIMENT

A bench top experiment was developed to screen promising membrane materials and to provide data for model validation (Figure 9). Two chambers, of 0.002 m^3 volume each, were separated by a $1/2$ or $3/8$ inch thick test membrane held in an acrylic frame (Figure 10). The frame was bolted between flanges on the boxes, so that the test membrane could be easily replaced. The joints between the flanges and the frame were sealed by closed cell foam gaskets. The humidity levels and temperature were recorded every five minutes by Omega HX93AV-D humidity and temperature transducers. The transducers accuracies were 2.5% relative humidity and $0.6 \text{ }^\circ\text{C}$ for temperature. In addition the temperature was measured in each test chamber with type T thermocouples with an accuracy of $1 \text{ }^\circ\text{C}$. A standard DC power supply applied voltage to the electrodes on each side of the membrane.

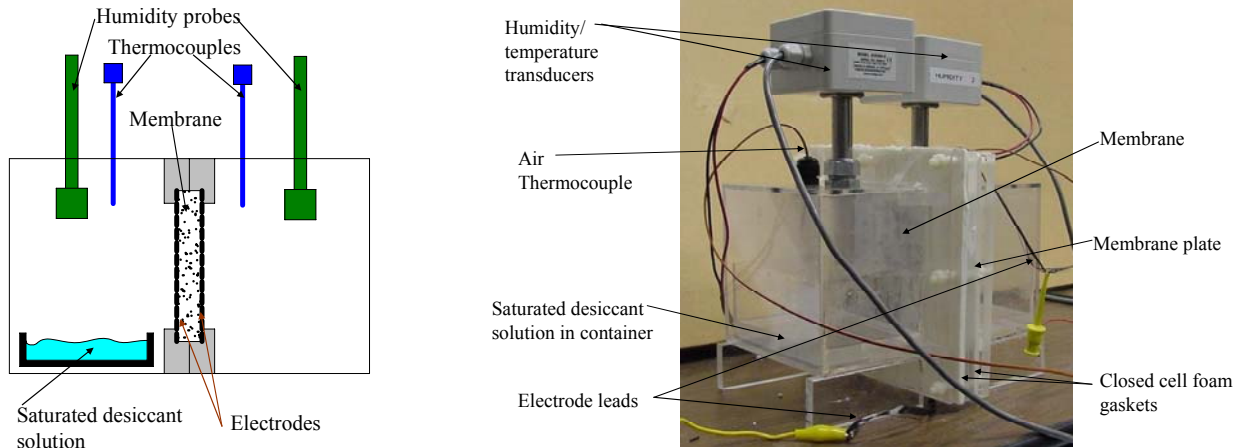


Figure 9: Left: Schematic of free convection membrane experiment Right: Free convection setup with silica gel concrete membrane

A saturated salt solution held one side of the membrane at a set humidity. Both sodium chloride and calcium chloride solutions were used in experiments. The humidity in the other chamber was allowed to vary to demonstrate the electroosmotic dehumidification effect.

The water flow rate was determined from the change in humidity of the side with no desiccant solution. Because the flow rate in the tests was low, no liquid water was observed exuding from the membrane. The water simply evaporated off of the membrane backside and entered the air. If water vapor was pumped to the side with the desiccant it was absorbed into the solution.

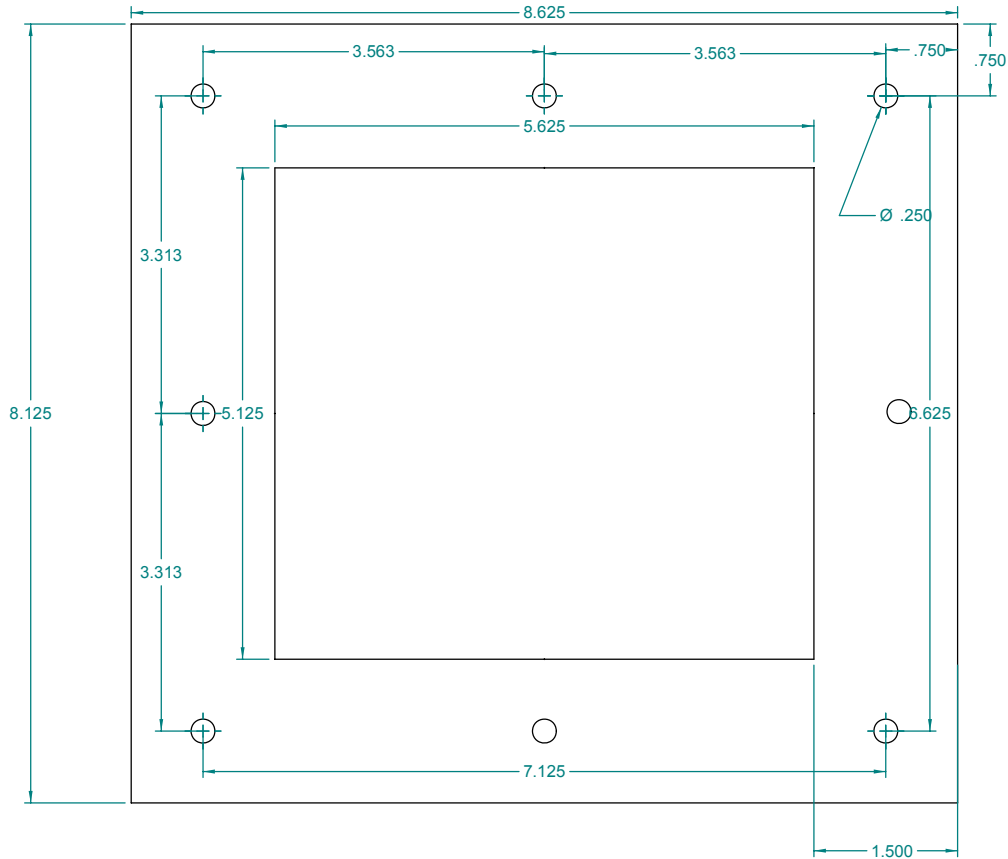


Figure 10: Drawing of acrylic frame that holds the membrane. Dimensions are in inches.

In the first sets of experiments the air in the chambers was not blown or mixed and the movement of water to and from the membrane was solely by diffusion. Concentration driven free convection was probably insignificant. In later tests, a small fan (4.5 cfm) was added to each chamber to reduce the convective mass transport resistance. The fans were attached at the vertical midpoint of the back wall and pointed down. After the addition of fans, the humidity equilibrated faster at the level determined by the salt solution. However, no improvement in the rate of electroosmotic transport was noted. Leakage through the gaskets may have increased with the fans, thus reducing the effect.

INORGANIC MEMBRANE EXPERIMENTS

A variety of membrane materials based on silica gel, Plaster of Paris, or zeolites were investigated. These will be termed inorganic materials, although some of the membranes contained polymers such as agar.

The most successful inorganic membrane was a silica gel concrete using Plaster of Paris as the cement and silica gel particles as the aggregate (Figure 11). After the mixture hardened, the surface was sanded back to expose the silica gel particles to the air. Carbon fiber strands were laid serpentine on the membrane faces and glued to the surface with Plaster of Paris to act as the electrode. The electrode current conductors must be closely spaced to produce an even current distribution. However, they should not obstruct the water vapor from adsorbing into the membrane surface.



Figure 11: Left: Photo of sanded surface with coarse silica gel Right: Micrograph of silica gel concrete

A container of saturated NaCl solution in the chamber on one side of the membrane maintained the air at 73% relative humidity. Without any forced convection, the time for diffusion through the air to reach equilibrium is on the order of days (Figure 12). The water diffused through the membrane and caused the other side to also trend towards this equilibrium value.

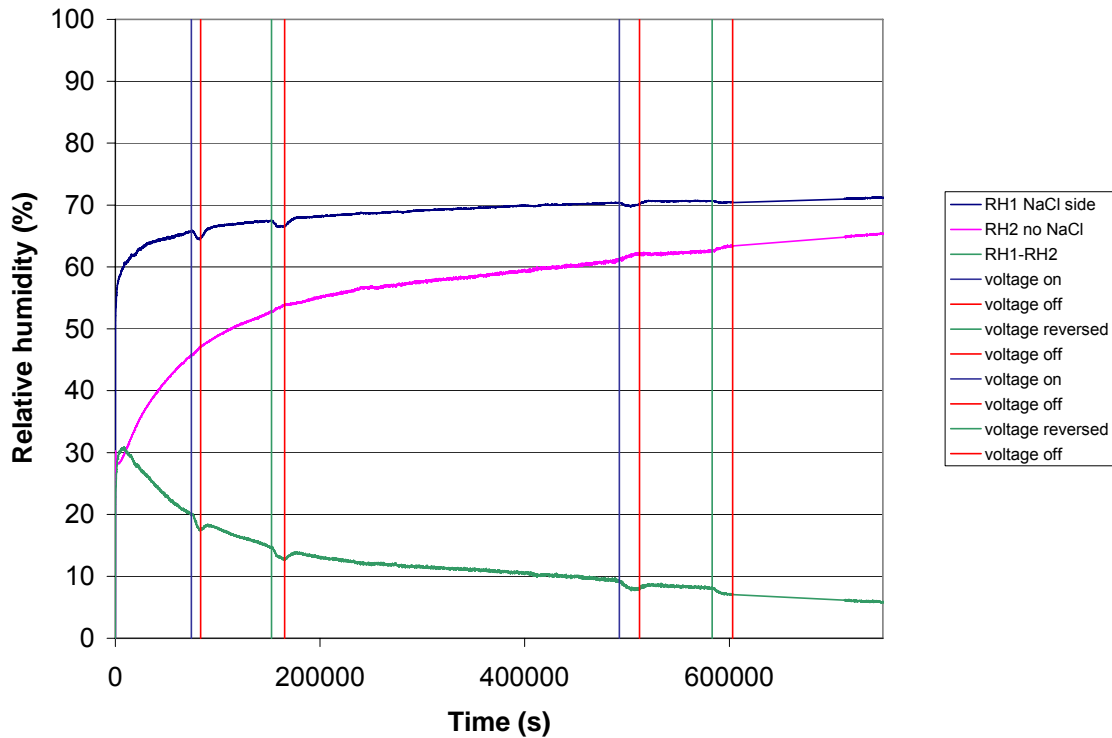


Figure 12: Time series data of plaster membrane experiment. Blue line is the relative humidity on the side with NaCl, pink line the relative humidity on the side with no solution, and the green line the difference in the relative humidity between the two sides. Vertical lines show the times when the current was turned on or off.

This test demonstrated humidity changes with the application of voltage. However, the humidity changes are comparable to the stated instrumentation error. The total moisture flow was insufficient to give signal strong enough for forced convection tests. The measured molar flux is in the range of 10^{-9} - 10^{-7} mol/s- m^2 .

Contrary to the expected behavior, the direction of the humidity change was not dependent on the polarity of the applied voltage. This may be due to the combination of opposite flow directions in the membrane components. The Plaster of Paris acts as a base and the silica gel acts as an acid. Therefore the two membrane components should have opposite zeta potentials and the flow in each component should be in opposite directions (Figure 13).

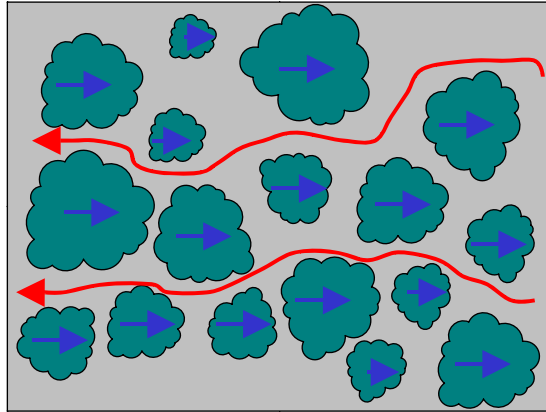


Figure 13: Water may flow one direction in silica gel particles and the other direction in the plaster matrix.

Appendix C describes other inorganic-based membrane materials that were investigated.

NAFION[®] MEMBRANES

Nafion[®] is a sulfonated tetrafluoroethylene copolymer produced by DuPont. Because of its chemical resistance and ability to conduct protons (H^+ ions), it is commonly used as the membrane in polymer electrolyte membrane (PEM) fuel cells.

Nafion[®] is also used in diffusion driven membrane dryers for gases (Ye 2003, Yang et al. 1996). These operate in a similar manner to total enthalpy exchangers, but usually have much smaller flow rates and are used in such applications as spectroscopy.

PROTON CONDUCTING POLYMER MEMBRANE MODEL

Although the model for silica gel membranes developed in Phase 1 and improved in Phase 2 could be adapted to model organic polymer membranes, a new model of proton conducting polymer membranes was developed during Phase 2, because the methods used to model water transport in fuel cell membranes use a different formulation and a different set of property data are reported in the literature.

Electroosmotic Flux Calculation

In fuel cell modeling the flux of water molecules is commonly assumed to be directly proportional to the flux of ions. The ratio of H^+ ions passing through the membrane to water

molecules transported is termed the electroosmotic drag coefficient. Zawodzinski (1995) measured a value of 1 for vapor equilibrated membranes. The molar flux due to electroosmosis ($\text{molar}_{\text{flux,eos}}$) is calculated by:

$$\text{molar}_{\text{flux,eos}} = \text{transference}_{\text{num}} \cdot \frac{i}{9.649\text{E}+07 \text{ [Coulomb/kmol]}}$$

where $\text{transference}_{\text{num}}$ is the electroosmotic drag coefficient, the value in the denominator is the Faraday constant, the ratio of the number of electrons in a Coulomb to the number of particles in a kilomole, and i is the current density in Amp/cm^2 .

The conductivity of the membrane was calculated by the following empirical formula developed by Sone (1996) for Nafion[®] 117 at 20°C without treatment (E form):

$$\text{NAFION}_{\text{cond}} = a + b \cdot (\text{RH}_{\text{in}} \cdot 100) + c \cdot (\text{RH}_{\text{in}} \cdot 100)^2 + d \cdot (\text{RH}_{\text{in}} \cdot 100)^3$$

$$a = -19.8\text{e-}3$$

$$b = 16.6\text{e-}4$$

$$c = -34.5\text{e-}6$$

$$d = 28.4\text{e-}8$$

where $\text{NAFION}_{\text{cond}}$ is the conductivity of Nafion[®] in $1/\text{cm}\cdot\Omega$, and RH_{in} is the relative humidity as a fraction (0 to 1). The resistance per unit area (R_{area}) is calculated by dividing the membrane thickness by the conductivity:

$$R_{\text{area}} = \frac{\text{thickness}}{\text{conductivity}}$$

The membrane thickness for the modeling is 15 mils or 381 μm . The voltage drop due to resistance in the electrodes on each side of the membrane is negligible. The total current-voltage relationship is:

$$i = \frac{V}{R_{\text{area}}}$$

Because the electroosmotic flux sets up a concentration gradient, a diffusional flux flows in the opposite direction. This molar flux ($\text{molar}_{\text{flux,diffusion}}$) is calculated by:

$$\text{molar}_{\text{flux,diffusion}} = -D_{\text{diffusion}} \cdot \left[\frac{C_{\text{H}_2\text{O},1} - C_{\text{H}_2\text{O},2}}{\text{thickness}} \right]$$

where $C_{\text{H}_2\text{O},1}$ and $C_{\text{H}_2\text{O},2}$ are the molar concentrations on both sides of the membrane. The diffusion coefficient ($D_{\text{diffusion}}$) is the average of the diffusion coefficients in cm^2/sec on each side

of the membrane. They are calculated from data in Burnett et al (2006) for the diffusion coefficient of water in Nafion[®] 117 as a function of relative humidity. The molar fluxes can be diverted into the mass fluxes by multiplication by the molecular weight of water (MW_{H_2O}). The total mass flux of water is:

$$\text{mass}_{\text{flux,diffusion}} = \text{molar}_{\text{flux,diffusion}} \cdot MW_{H_2O}$$

The total mass flow rate through the membrane is equal to the dehumidification requirement. This determines the total surface area of the membrane for a given applied voltage or the voltage that must be applied for a given surface area.

Model Results

The modeling results are in a range that is realistic for practical use. The current densities are on the order of tens of milliamps per square centimeter. The voltage is also in the range of tens of millivolts across a single membrane. A real system may electrically connect membranes in parallel in order to increase the voltage required. The mass fluxes are on the order of 10^{-9} kg/s-cm².

Membrane Thickness

As the membrane thickness increases the electrical resistance increases. At the same time the back diffusion of water decreases (Figure 14). Therefore a thicker membrane can maintain a larger vapor pressure difference, but at a reduced pumping efficiency than a thinner membrane. Alternatively total mass flux through a membrane increases with increasing membrane thickness when the humidity conditions on each side of the membrane are held constant (Figure 15).

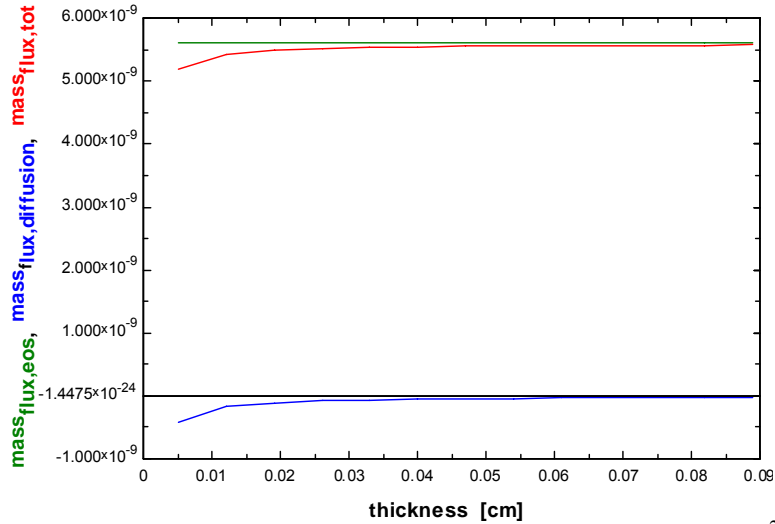


Figure 14: The electroosmotic, diffusion, and total water mass fluxes ($\text{kg/s}\cdot\text{cm}^2$) through the membrane versus thickness for set humidity conditions ($\text{RH}_1=0.775$, $\text{RH}_2=0.715$, $i=30\text{mA/cm}^2$). The label colors correspond to the lines on the graph.

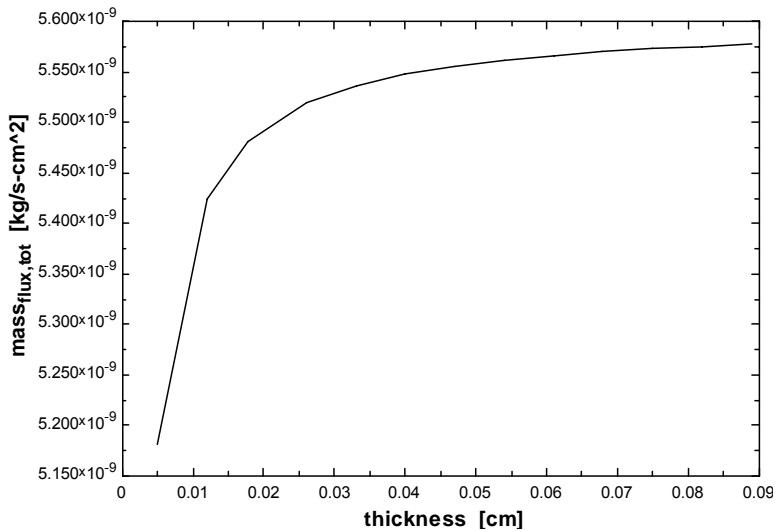


Figure 15: The total water mass flux through the membrane increases with increasing thickness for set humidity conditions ($\text{RH}_1=0.775$, $\text{RH}_2=0.715$, $i=30\text{mA/cm}^2$)

Because this model uses the average water content of the two sides to calculate the conductivity, the membrane resistance increases linearly with membrane thickness for constant humidity conditions. Consequently, the energy required per unit mass to pump the water is linearly related to membrane thickness (Figure 16).

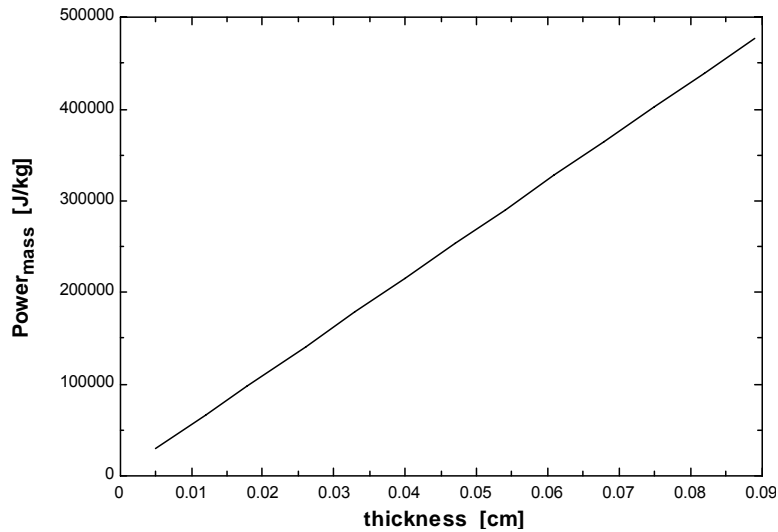


Figure 16: The energy expended to pump a unit mass of water increases with increasing thickness for set humidity conditions ($RH_1=0.775$, $RH_2=0.715$, $i=30\text{mA}/\text{cm}^2$)

NAFION[®] MEMBRANE EXPERIMENTS

The performance of Nafion[®] membranes was tested in the same manner as the inorganic membrane tests described above. However the Nafion[®] membranes are 10x10cm and have a smaller area than the inorganic membranes. A Nafion[®] 117 membrane electrode assembly (MEA) with commercially applied fuel cell electrodes and catalysts was used. The Nafion[®] membranes were mounted between acrylic frames with polyethylene sheet gaskets and mounted in the two chamber setup described above. Stainless steel mesh current collectors were mounted in contact with the membrane faces. The fans were on throughout all Nafion[®] tests.

A regulated electrical power supply applied a constant current to the membrane. Currents of 1, 2, 3, and 10 amps were used. This corresponds to current densities of 0.01, 0.02, 0.03, and 0.10 amp/cm^2 . Jeon (2006) reported a long term degradation in membrane performance with increasing current density in direct methanol fuels cells. At current densities of 100, 150, and 200 mA/cm^2 after a period of 145 hours, the fuel cell power densities were 93.9, 79.9, and 55.1% of the initial value. Consequently, the maximum current density used in the experimental tests was set at 100 mA/cm^2 or 10 amps total for the test setup. However, the membrane performance dropped dramatically after this test and the membrane may have been damaged.

The humidity on one side of the membrane was kept constant with saturated NaCl solution ($RH \sim 75\%$).

The time series data from these experiments was curve fit to determine the diffusion and electroosmotic coefficients (Figure 17 and 18). The humidity ratio increased on the side of the membrane with the saturated salt solution, because the temperature increased from the ohmic heating of the membrane (Figure 17). The electroosmotic flow is assumed to be directly proportional to the current. The diffusion rate is assumed to be directed proportional to the difference in humidity ratio across the membrane. At zero current, all flow through the membrane is assumed to be due to concentration driven diffusion.

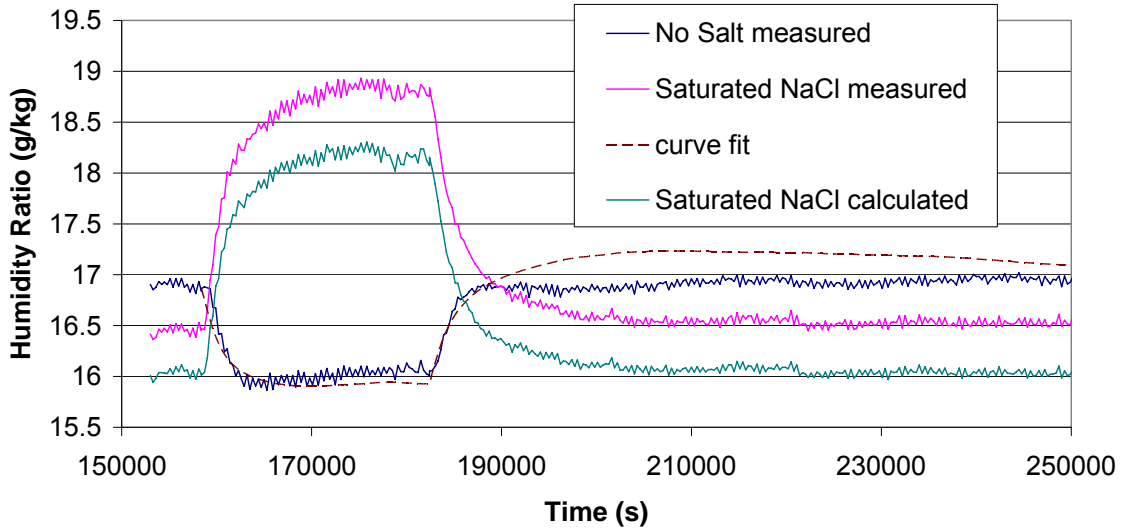


Figure 17: Time series data of humidity ratios for test at 3 amp current. Pink: Humidity ratio on the side of the membrane with saturated salt solution, Dark Blue: Humidity ratio on membrane side without salt, Teal: Equilibrium humidity ratio of saturated salt solution calculated from the air temperature. Brown dashed: Humidity ratio on side of membrane with no salt as calculated by the curve fit.

The proportionality constants are used as fitting parameters. The instantaneous diffusional flux is calculated from the measured humidity ratio values (ω_1 and ω_2) and the effect of total diffusion coefficient (D_{eff}):

$$m''_{\text{diffusion}} = D_{\text{eff}} (\omega_1 - \omega_2 - \omega_{\text{offset}})$$

The average difference between the readings from the humidity transducers at equilibrium with no applied current (ω_{offset}) was subtracted from the higher reading to adjust for any experimental

error offset. The convective resistance from the bulk flow to the surface is also included in the measured diffusion coefficient. The electroosmotic flux (m''_{eos}) is calculated by:

$$m''_{eos} = C_{eos} I$$

where C_{eos} is the effective electroosmotic coefficient and I is the total current flow through the membrane. The total flow through the membrane is calculated by:

$$m''_{total} = m''_{eos} + m''_{diffusion}$$

The time series of the humidity on the side without the NaCl was calculated from these formulas. The initial value for the humidity was taken from the experiment shortly before the current was turned on, when the humidity levels on both sides of the membrane had reached diffusion equilibrium and were steady. The predicted humidity value at the next time step (ω_{j+1}) is predicted from the value at the current time step (ω_j) by:

$$\omega_{j+1} = \omega_j + \Delta t \cdot m''_{total}$$

where Δt is the time between measurements. The electroosmotic and diffusion coefficients were determined through a combination of minimizing the sum of the squared errors and subjective manual fitting to the graphs.

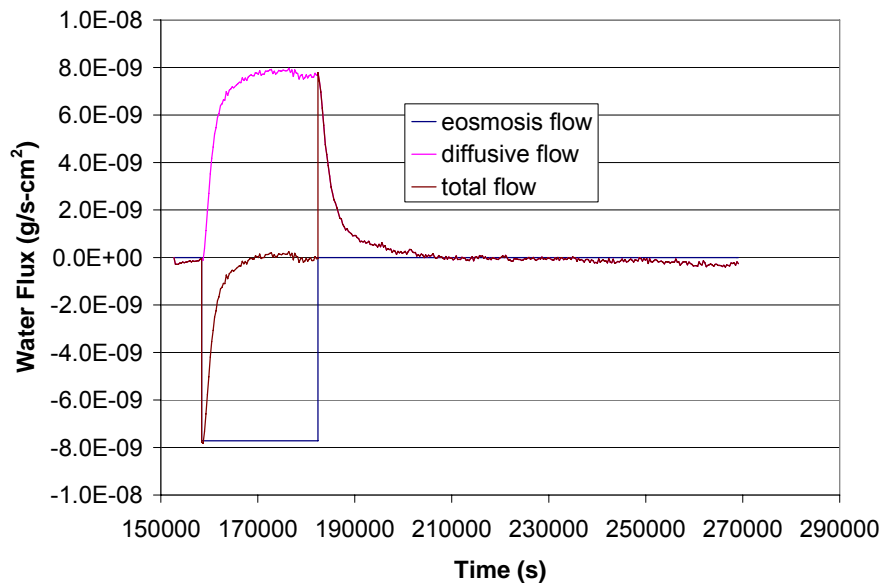


Figure 18: Electroosmotic and diffusion flows at 3 amp current as determined from the curve fit to experimental data. (Note: The flux in the graph is in units of g not kg)

Comparison of Experiment to Model

The diffusion flux is similar in magnitude to that predicted by the model. However, the electroosmotic flux is three orders of magnitude smaller than that predicted (see modeling comparison below).

The measured electroosmotic flow through the membranes in the test was about 1000 times smaller than that predicted by the model. The measured resistance of the membrane is an order of magnitude larger than that predicted from published data for the same humidity levels. The energy expended per unit mass is approximately 10000 times that predicted. The measured back diffusion rate is an order of magnitude lower than predicted. However, the raw humidity measurements were of similar magnitude to the measurement accuracy. In addition, the results of the curve fitting technique are very sensitive to the data.

Using a thicker Nafion[®] membrane should demonstrate a larger humidity change (see modeling section on membrane thickness), allowing a greater certainty about the magnitude of the results.

COMPARISON TO PRESENT TECHNOLOGY SYSTEM MODELING

The performance of an air conditioning system using an electroosmotic dehumidification system in series with a conventional vapor compression cycle was modeled. The electroosmotic system handles the entire latent load and the vapor compression system handles the entire sensible cooling load (Figure 19 and 20). Performance of the system was compared to a conventional vapor compression air conditioner that handles both the latent and sensible loads with a single evaporator coil. A block diagram of the model structure is shown in Figure 21.

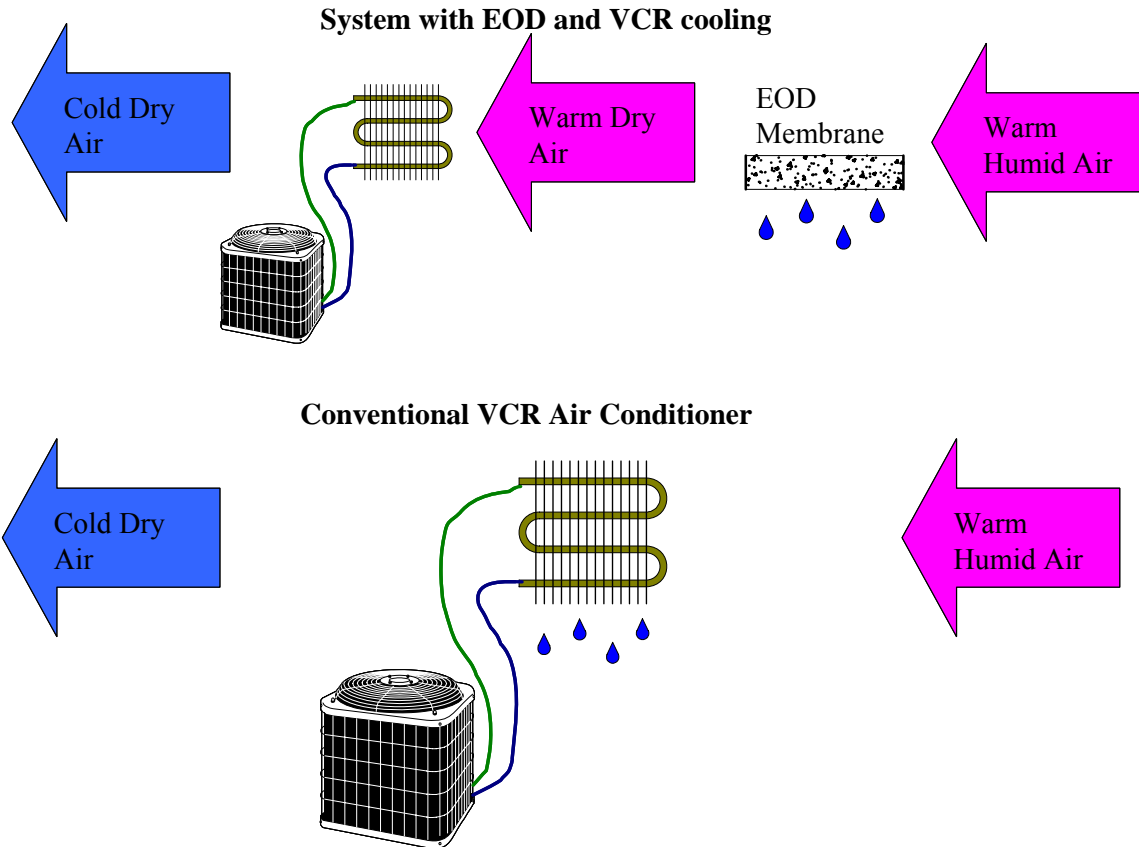


Figure 19: Top: Electroosmotic dehumidification membrane in series with a conventional vapor compression cycle air conditioner. Bottom: A conventional vapor compression air conditioner handling both the latent and sensible loads. Note: the water leaving the electroosmotic dehumidification membrane may leave as vapor, not as the water droplets depicted in the schematic.

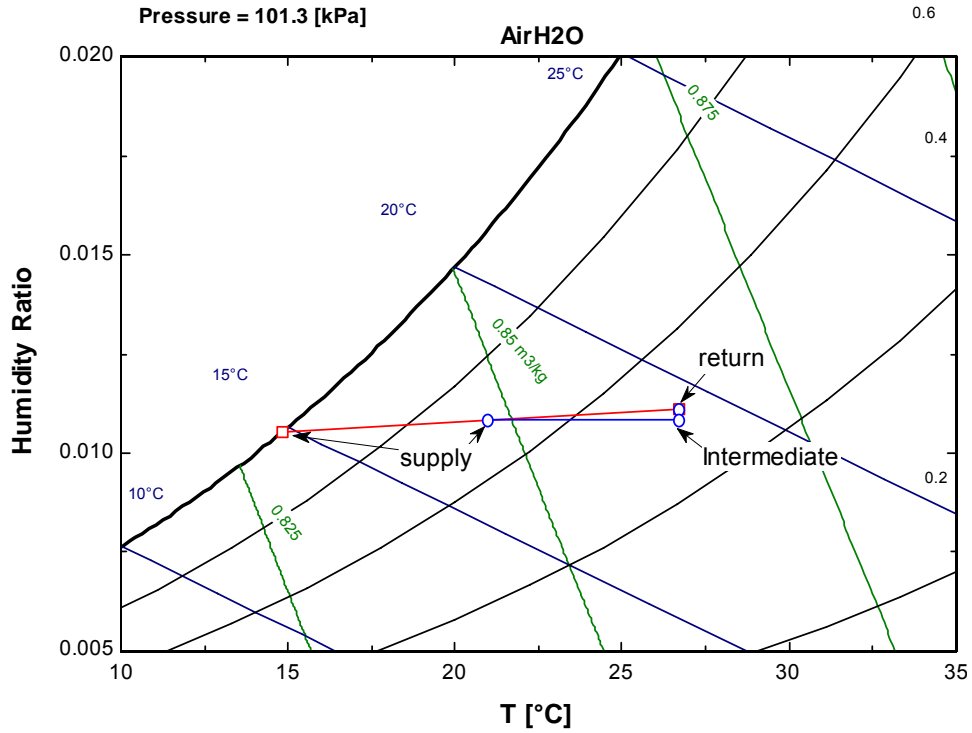


Figure 20: Process paths of conventional vapor compression air conditioning (red squares) and electroosmotic dehumidification followed by sensible cooling (blue circles).

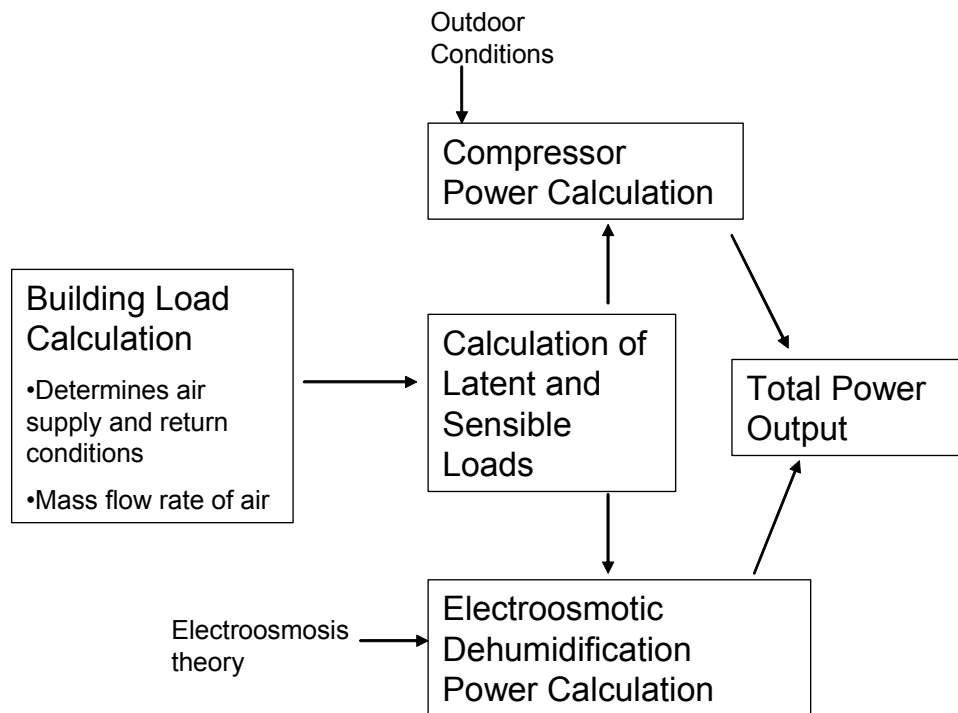


Figure 21: Flow chart of calculation of energy use by an electroosmotic humidifier in series with a vapor compression air conditioner.

The latent and sensible loads for the base case were calculated for a 250 m² residence by a similar method to Mina (2004). However, the ARI rating conditions for unitary equipment (ARI, 2006) were used for the entering airflow and the outside conditions. The return air entering the indoor section of the air-conditioning system is at 26.7 °C dry bulb temperature and 19.4 °C wet bulb temperature. The outside air conditions are 35.0 °C dry bulb and 23.9 °C wet bulb temperature. The building has 6 occupants generating a total of 0.5 kg/hr of moisture. The moisture infiltration rate is 1 kg/hr per kPa of humidity partial pressure difference. The sensible load is 5.75 kW. This is the same value per square meter of finished area as the example house in chapter 29 of the 2005 ASHRAE Handbook: Fundamentals.

Process Air Conditions

The air mass flow through the electroosmotic system can be varied, because the latent and sensible loads are decoupled. The dehumidification load ($Latent_{tot}$) is related to the supply (ω_{supply}) and return (ω_{return}) humidity ratios and the mass flow rate of dry air by:

$$Latent_{tot} = \dot{m}_{dry\ air} \cdot (\omega_{supply} - \omega_{return})$$

The sensible load is calculated as the difference in enthalpy of dry air flows at the supply and return temperatures. The air exiting the traditional air conditioning system is assumed to be saturated at a relative humidity of 1. Therefore, the air flow is uniquely determined by the latent and sensible loads (or sensible heat ratio).

Vapor Compression Cycle Efficiency

The efficiencies of the vapor compression cycles used in the traditional system and for the sensible cooling in the electroosmotic dehumidification system are calculated with the same subroutine. The condenser and evaporator exit temperatures are set at the outside and supply air temperatures respectively. No superheating or subcooling is assumed. The compressor is assumed to have an isentropic efficiency of 0.5.

COMPARISON TO PRESENT TECHNOLOGY SYSTEM RESULTS

For given size membrane, as the airflow is increased the electroosmotic flux through the membrane does not change, because the latent load does not change. However, the supply air temperature increases to maintain the same sensible cooling power. This corresponds to an

increase in the evaporator temperature and an increase in COP (Figure 22). However in a real system the fan power would increase with the flow rate, counteracting this increase in COP. Because the airflow in the present technology system does not vary for set load conditions, it has a constant COP. For an appropriate selection of membrane size, voltage, and airflow, the predicted COP of the combined system is higher than the present technology system. In a real system the increase in fan power with increased air flow rate would limit this COP increase.

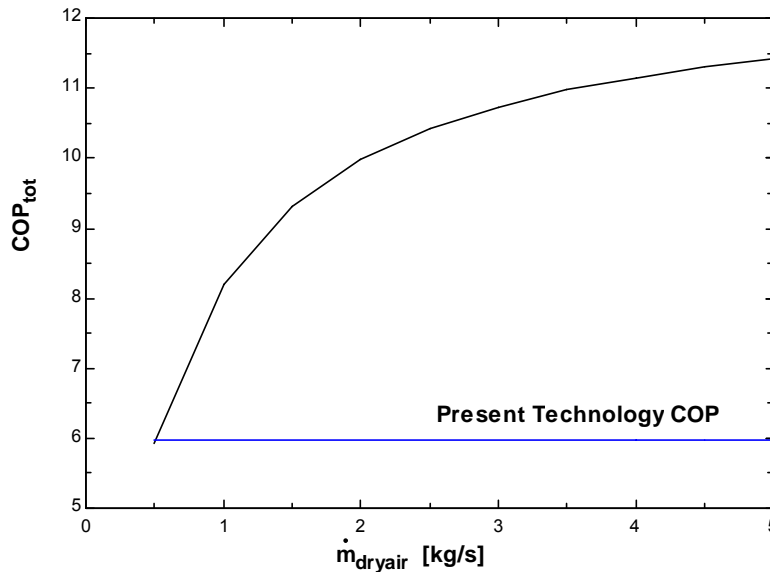


Figure 22: COP of the electroosmotic system as a function of air mass flow rate compared to the present technology system for the same load conditions ($V=0.1$, $Area_{membrane}=5 \text{ m}^2$, $i=30\text{mA/cm}^2$)

Membrane Surface Area

There is a size versus efficiency tradeoff in electroosmotic dehumidification systems. As with a heat exchanger, the efficiency of the mass transfer through the device increases with surface area at a given air flow rate. The efficiency of most electrochemical devices increases with an increase in surface area (Gerlach 2003 and 2004). For a given latent load the total current is constant. Increasing the surface area corresponds to a decreased current density and therefore lower voltage and power input (Figure 23). The power input is linearly related to the voltage, leading to an increase in the COP with area (Figure 24).

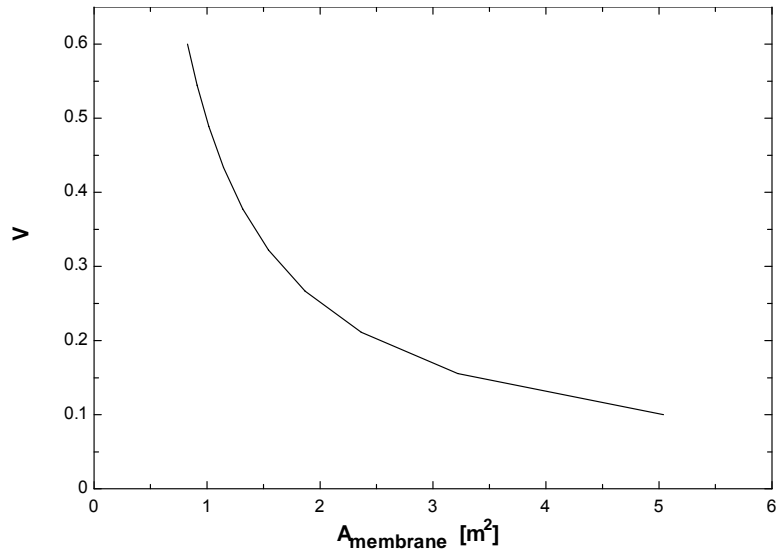


Figure 23: At a set humidity load, as the membrane area increases the voltage decreases (Airflow 3 kg/s).

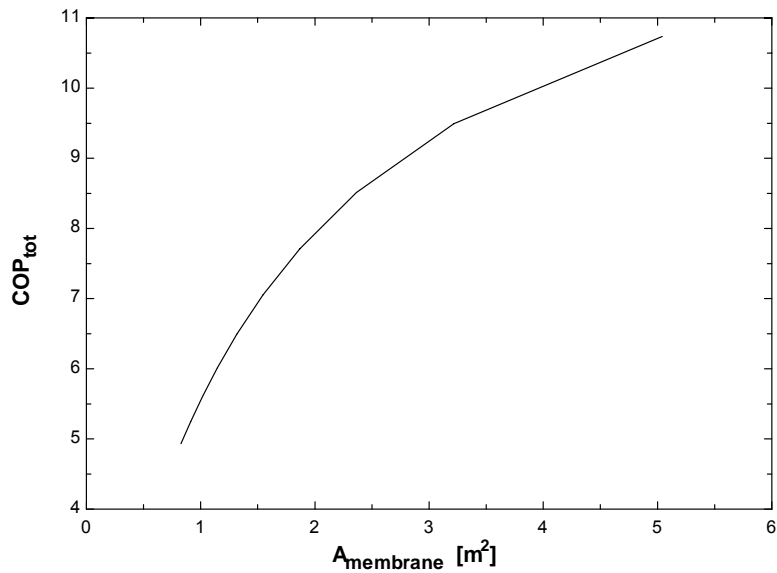


Figure 24: The COP increases with area (Airflow 3 kg/s).

The predicted membrane size of less than 10 m² for a residence is quite realistic. This area could easily fit as a series of parallel membranes in an air handling unit similar to designs for membrane total enthalpy exchangers.

At this time the capital and maintenance costs of electroosmotic dehumidification equipment may be hard to assess. However, the use of the electroosmotic dehumidification

system may allow a smaller vapor compression air conditioning system to be used in climates where dehumidification is a major component of air conditioning.

Adjustment for Experimental Results

Many of the parameters measured in the membrane experiments are several orders of magnitude different than that predicted by the model implying that a real system would have performance considerably less than that predicted. However, the experimental error in the experiments was so large that it is unclear how much of a difference from the predictions could be expected.

APPORTIONMENT OF SORPTION AND OHMIC HEAT

In typical solid desiccant configuration the heat of absorption is rejected to the air stream that is being dried. This increases the air temperature and the cooling load required of the refrigeration cycle. In electroosmotic dehumidification the absorption and desorption processes occur on opposite sides of a thin membrane. It is unclear a priori if the heats of absorption and desorption are exchanged with the process and moisture removal airstreams or are conducted through the membrane. In addition, the ohmic heat from the electrical current in the membrane must be rejected to the airstreams. Therefore the heat transfer within the membrane was modeled a simple quasi-one dimensional model of an infinite membrane (Figure 25) including the heat balance at the surface of the conduction, convection, and sorption energies.

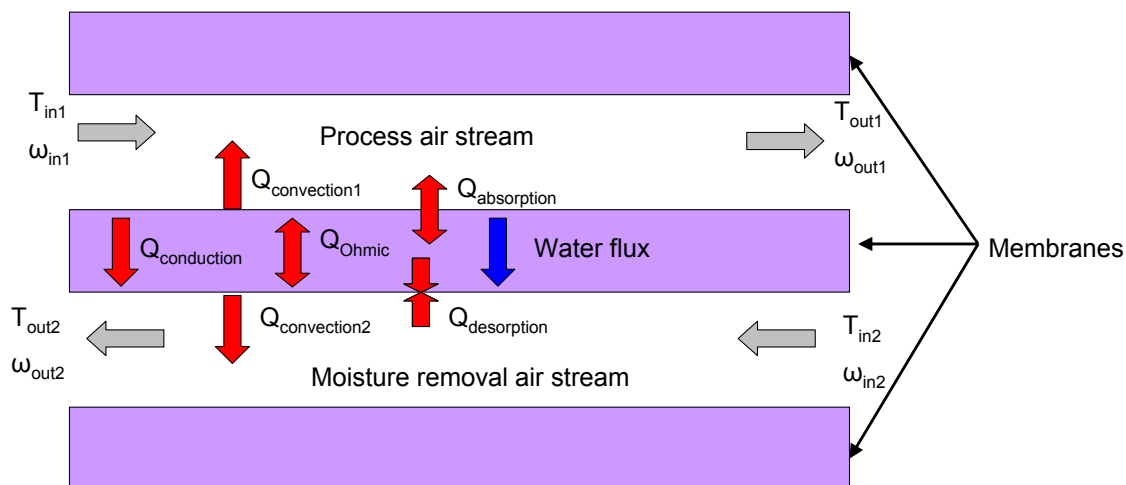


Figure 25: Schematic of heat flows in membrane model

The membrane itself is a plane wall with internal heat generation and constant temperature boundaries. The air on both sides of the membrane enters at 25°C.

The heat flux at the absorbing membrane surface is

$$0 = Q_{\text{conv},1} - Q_{\text{cond},1} + Q_{\text{absorb}}$$

where $Q_{\text{conv},1}$ is the convection heat transfer and Q_{adsorb} is the heat of absorption at the surface. Positive heat conduction ($Q_{\text{cond},1}$) is from the adsorption side towards the desorption side. The heat flux at the adsorbing membrane surface is

$$0 = Q_{\text{conv},2} + Q_{\text{cond},2} + Q_{\text{desorb}}$$

$$0 = Q_{\text{conv},1} - Q_{\text{cond},1} + Q_{\text{absorb}}$$

where $Q_{\text{conv},2}$ is the convection heat transfer and Q_{desorb} is the heat of desorption at the surface. Positive heat conduction ($Q_{\text{cond},2}$) is from the adsorption side towards the desorption side. The volumetric heat generation rate (q_{gen}) is computed by:

$$q_{\text{gen}} = V \cdot \frac{i}{\text{thick}_{\text{memb}} \cdot \left| 0.0001 \cdot \frac{\text{m}^2}{\text{cm}^2} \right|}$$

where i is the current density (A/cm²). V is the applied voltage, and $\text{thick}_{\text{memb}}$ is the membrane thickness. The heat conducted to each membrane surface is calculated from the exact solution to heat conduction in a plane wall with constant temperature boundary conditions and internal heat generation. The heat conducted to the adsorption side is:

$$Q_{\text{cond},1} = -k_{\text{memb}} \cdot \left[\frac{T_{2,\text{surf}} - T_{1,\text{surf}}}{\text{thick}_{\text{memb}}} \right] - q_{\text{gen}} \cdot \frac{\text{thick}_{\text{memb}}}{2}$$

where k_{memb} is the membrane thermal conductivity. $T_{1,\text{surf}}$ and $T_{2,\text{surf}}$ are the surface temperatures.

The heat conducted to the desorption side is

$$Q_{\text{cond},2} = q_{\text{gen}} \cdot \text{thick}_{\text{memb}} - k_{\text{memb}} \cdot \left[\frac{T_{2,\text{surf}} - T_{1,\text{surf}}}{\text{thick}_{\text{memb}}} \right] - q_{\text{gen}} \cdot \frac{\text{thick}_{\text{memb}}}{2}$$

Although the heats of absorption and desorption vary in a real system due to the different humidity ratios and temperatures on the two sides of the membrane, they are roughly equivalent. For this model, they are both assumed to be equal to the latent heat of vaporizations (or condensation) of water at 1 atm and the respective surface temperature. The absorption and desorption energy changes occur in an infinitesimal surface layer.

The convective heat transfer is calculated assuming laminar heat transfer between infinite flat plates spaced 1 cm apart. The Nusselt number for constant surface heat flux is used due to the constant current condition and constant heat generation (Incropera, 1996, pg. 450).

The airside energy balance on the adsorption side is:

$$Q_{\text{conv},1} + Q_{\text{absorb}} = - (h_{1,\text{airout}} - h_{1,\text{airin}}) \cdot \dot{m}_{\text{air}} \cdot \frac{\left| 1000 \cdot \frac{\text{J}}{\text{kJ}} \right|}{L_{\text{element}}}$$

where $Q_{\text{conv},1}$ is the convection heat transfer and Q_{absorb} is the heat of sorption. $h_{1,\text{airout}}$ and $h_{1,\text{airin}}$ are the air enthalpies entering and exiting the membrane section. L_{element} is the length of the membrane section. The airside energy balance on the desorption side is:

$$Q_{\text{conv},2} + Q_{\text{desorb}} = - (h_{2,\text{airout}} - h_{2,\text{airin}}) \cdot \dot{m}_{\text{air}} \cdot \frac{\left| 1000 \cdot \frac{\text{J}}{\text{kJ}} \right|}{L_{\text{element}}}$$

The convective resistance from the membrane surface to the air is higher than the conductive resistance through the thin membrane. Therefore, the energy released by the absorption process is conducted through the membrane and consumed in the desorption process. If the airstreams enter at the same temperature, the exit temperatures are very close and are determined by the ohmic heat generation and not the sorption processes. In addition, if the temperature streams enter at different temperatures the heat conduction through the membrane can be significant, similar to a membrane energy recovery ventilator.

Figure 26 shows the effect of membrane thickness on the temperatures of the exhaust air for constant applied voltage and current. In this unrealistic condition the membrane thickness does not affect the power dissipated. Consequently, as the membrane thickness increases the average membrane temperature does not vary. The average temperature is slightly offset above the inlet temperature of 25°C. As the membrane thickens the temperatures diverge due to the increased conduction resistance, eventually reaching an asymptote.

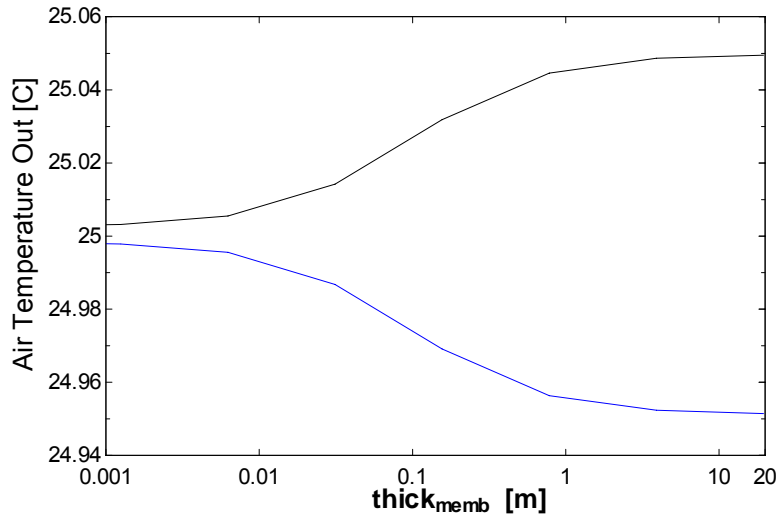


Figure 26: Temperature of air streams leaving device as a function of membrane thickness for constant ohmic heat flux. The adsorption side is shown in black and the desorption side in blue.

For a situation where the current is kept constant and the membrane resistance increases with thickness (Figure 27), the average temperature of the exiting streams increases linearly due to the linear increase in resistance with thickness. The temperatures on the two sides diverge as before. Figure 27 does not cover the same range as Figure 26 because the surface temperature exceeds the boiling point of water.

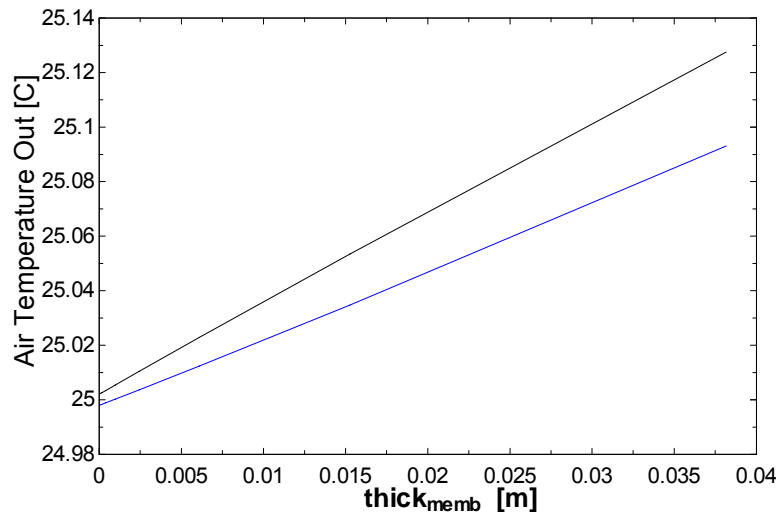


Figure 27: Temperature of air streams leaving device as a function of membrane thickness when resistance varies with thickness. The adsorption side is shown in black and the desorption side in blue.

RECOMMENDATIONS FOR FUTURE WORK

Experiments with thicker membranes should demonstrate a larger humidity change, allowing a greater certainty about the magnitude of the results. In addition, different membrane materials could be investigated. Other cross linked sulfonated polymers could potentially material replace Nafion[®] at a lower cost. Further research will be needed on the effect of fouling on the membranes.

CONCLUSIONS

Modeling based on the published properties for Nafion[®] indicates the feasibility of electroosmotic dehumidification for separating the control of latent and sensible load in air conditioning systems. The total COP of the system, neglecting fan power, can be 1-2 times higher (depending on airflow rate) than a system using an evaporator for latent and sensible load. Experiments with Nafion[®] membranes demonstrated an electroosmotic effect. However, the flux was several orders of magnitude lower than that predicted by the model. Further research is needed to reconcile the experimental data and modeling in order to determine feasibility.

REFERENCES

- Anappara, Aji A., Swapankumar Ghosh, S. Rajeshkumar, P. Mukundan, P.R.S. Warriar, and K.G.K. Warriar. "Impedance spectroscopic studies of solgel derived subcritically dried silica aerogels." *Acta Materialia* 52(2) 369-375, 2004.
- American Society of Heating, Refrigeration, and Air-Conditioning Engineers, Inc. 2005 *ASHRAE Handbook: Fundamentals*.
- ARI (Air-Conditioning and Refrigeration Institute). *Standard for Performance Rating of Unitary Airconditioning and Airsource Heat Pump Equipment: Standard 210/240*. 2006.
- Burnett, Daniel J., Armando R. Garcia, and Frank Thielmann. "Measuring moisture sorption and diffusion kinetics on proton exchange membranes using a gravimetric vapor sorption apparatus." *J. Power Sources* 160: 426-430, 2006
- Gerlach, David W. *An Investigation of Electrochemical Methods for Refrigeration*. Doctoral dissertation, University of Illinois, Urbana-Champaign, 2004.

- Gerlach, David W. "Electro-osmosis for Dehumidification: Phase 1 Report." *ARTI Research Program*. Report No. ARTI -614-10090-01, May 2006. Available at http://www.arti-research.org/ARTI_Research_Reports.php
- Gerlach, D. W. and T. A. Newell. "Direct Electrochemical Method for Cooling and Refrigeration." *Proceedings of the 21st IIR International Congress of Refrigeration*, 17-22 August 2003, Washington, D.C.
- Greenspan, Lewis. "Humidity Fixed Points of Binary Saturated Aqueous Solutions." *Journal of Research of the National Bureau of Standards*, Section A, Physics and Chemistry, 81A(1), 89-96, Jan-Feb, 1977.
- Incropera, Frank P. and David P. Dewitt. *Fundamentals of Heat and Mass Transfer*, 4 ed. Wiley: New York, 1996.
- Jeon, Min Ku, Ki Rak Lee, Kwang Seok Oh, Dae Sik Hong, Jung Yeon Won, Shuang Li and Seong Ihl Woo. "Current density dependence on performance degradation of direct methanol fuel cells" *Journal of Power Sources*. 158(2) 1344-1347, 25 August 2006.
- Mina, E.M. *Dehumidification Effect by Coupling an Electroosmotic Material with a Desiccant Interface*. Ph.D. dissertation, University of Illinois at Urbana-Champaign, 2004.
- Mina, Ehab M. and Ty A. Newell. "Electroosmotic Dehumidification." *Proceedings of the 21st IIR International Congress of Refrigeration*, Washington, D.C., August 17-22, 2003.
- Pivovar, Bryan S., William H. Smyrl, and Edward L. Cussler. "Electro-osmosis in Nafion 117, polystyrene sulfonic acid, and polybenzimidazole." *Journal of the Electrochemical Society* 152(1) A53-A60, 2005.
- Sarioglu, Kemal and Tuba Kartal. "A Dryer." *World Intellectual Property Organization*, International Publication Number WO 2007/099109 A1, 7 September 2007.
- Sone, Yosbitsugu, Per Ekdunge, and Daniel Simonsson. "Proton Conductivity of Nafion 117 as Measured by a Four-Electrode AC Impedance Method." *J Electrochem. Soc.* 143(4) 1254-9, April 1996.
- Yang, Jinfu, Timothy S. Conner, John A. Koropchak, David A. Leighty. "Use of a multi-tube Nafion membrane dryer for desolvation with thermospray sample introduction to inductively coupled plasma-atomic emission spectrometry." *Spectrochimica Acta, Part B: Atomic Spectroscopy* 51B(12) 1491-1503, Oct. 1996.

Ye, Xinhuai, and M. Douglas LeVan. "Water transport properties of Nafion membranes: Part I. Single-tube membrane module for air drying." *Journal of Membrane Science* 221(1-2) 147-161, Aug 15, 2003.

Zawodzinski, Thomas A., John Davey, Judith Valerio, and Shimshon Gottesfeld. "Water content dependence of electro-osmotic drag in proton-conducting polymer electrolytes." *Electrochimica Acta* 40(3) 297-302, Feb. 1995.

APPENDIX A: INORGANIC MEMBRANE MATERIAL PROPERTY TESTS

A number of experiments were performed to attempt to determine the properties of the inorganic membrane materials. When the inorganic membrane tests were not successful, the property tests were halted and not completed.

An electrical conductivity measurement method for solid membrane materials was investigated. Ionic conductivity meters using high frequency AC must be used to reduce interference from electrode reactions. Initial attempts to measure the ionic conductivity of partially dried silica gels with a two-pin probe failed due to poor contact. It was proposed to make a conductivity cell out of standard size plastic tubing (see Figure A1). The conductivity cell constant would be calculated for each cell (Length/Area). Using two different cell lengths would allow the influence of contact resistance to be determined. A weighing scale would be used to measure the contact pressure applied from the electrodes.

In actual experiments there was a large variation in measured conductivity with applied force due to the compaction of the granular material. In addition, the shape of the conductivity cell had to be modified to a sample surface area of $>10\text{cm}^2$ due to the materials' low conductivity (Figure A1 right).

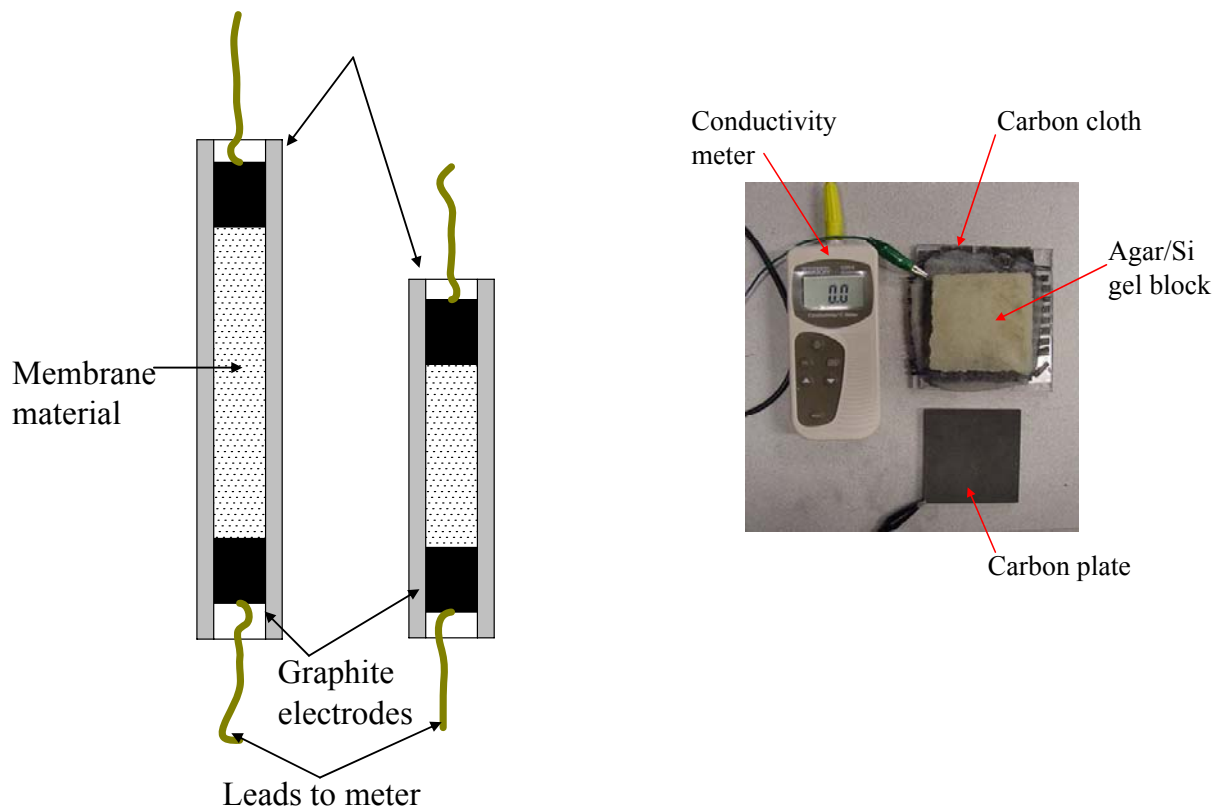


Figure A1: Left: Proposed conductivity measuring technique Right: Conductivity measurement test for agar-silica gel membrane

Modifications to the streaming potential apparatus were begun. A new water source using hydrostatic pressure instead of air pressure was constructed (Figure A2). This increased safety by eliminating the pressurized water tank and decreased the time necessary for refilling the tank.

Planned modifications that were not performed included fixing the outlet tube position more accurately and replacing all parts other than water tank. This would eliminate ensure cleanliness and reduce contamination by eliminating silicone and epoxy and replacing them with polyethylene, polypropylene, and fluoropolymers.

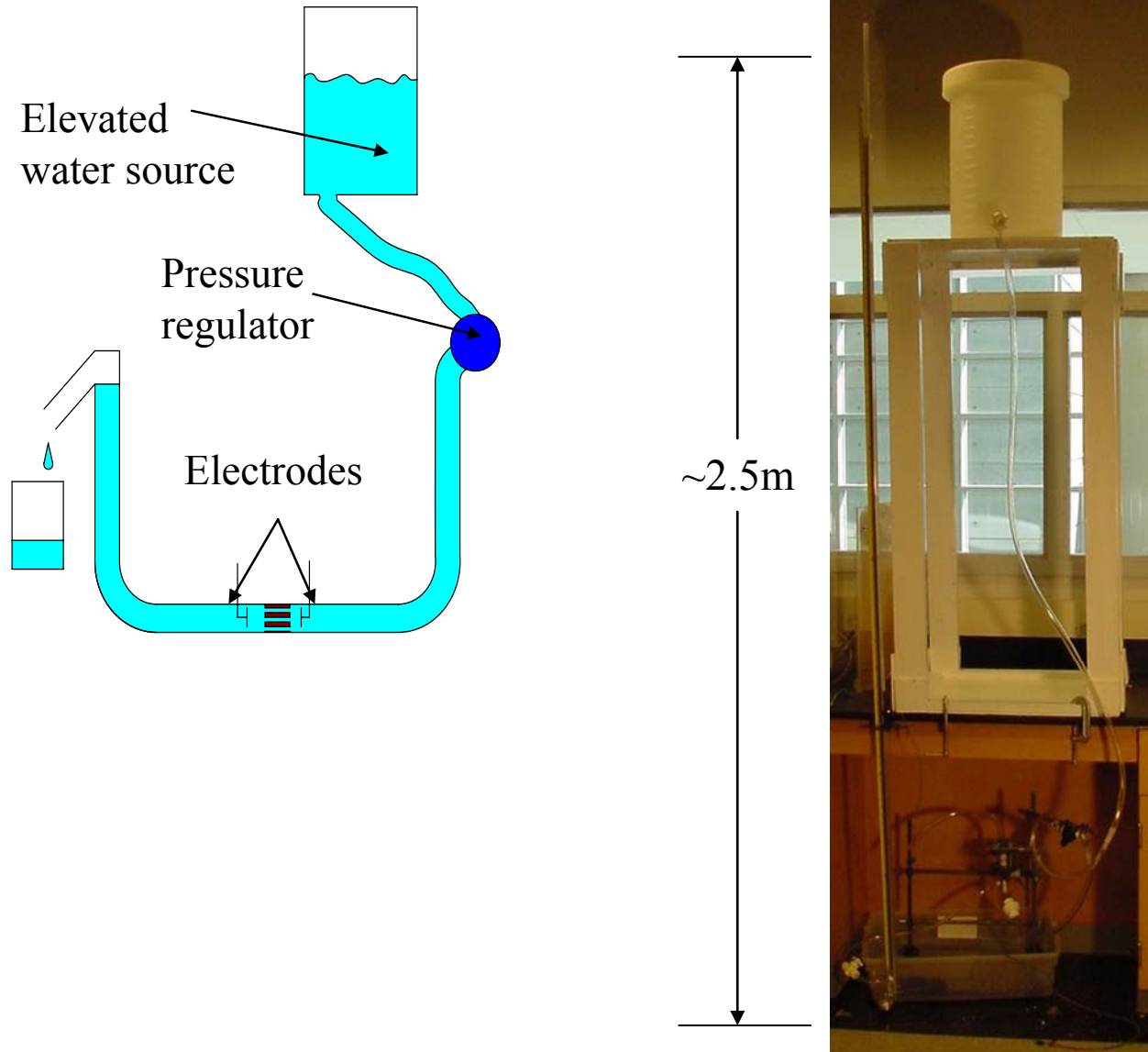


Figure A2: Phase 2 streaming potential experiment design Left: Schematic Right: Photograph of partially reconstructed setup

APPENDIX B: FORCED CONVECTION MEMBRANE EXPERIMENT

The forced convection membrane experiment proposed in the Phase 1 report was not performed because the low flow rate through the membrane would not give strong enough of a signal for measurement.

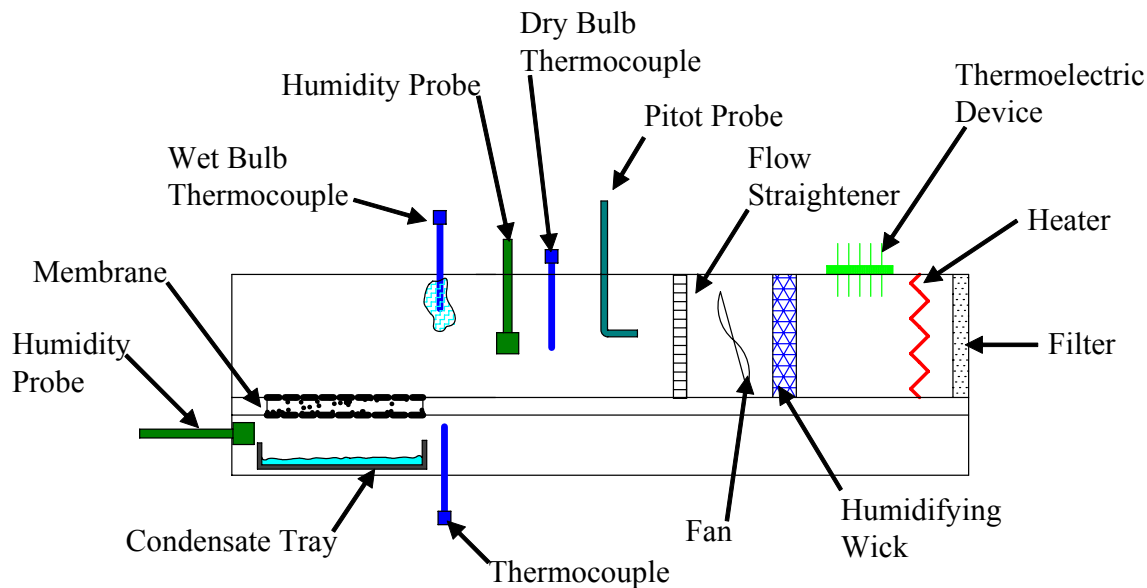


Figure B1: Schematic of proposed open loop forced convection membrane experiment

Moisture flow rate through membrane must be large enough to give a measurable signal. For example, using the one of the smallest off-the-shelf fans with a 4.5 cu/ft-min airflow and the same membrane size and flow rate from the tests, the change in humidity ratio is on the order of 10^{-8} /s.

A closed loop recirculating test could be performed. Because the same air would be passed over the membrane repeatedly, a small flow rate through the membrane would produce a measurable change in the humidity. However, a small leak of air into or out of the system could significantly affect the measurement accuracy.

APPENDIX C: OTHER INORGANIC MATERIALS INVESTIGATED

A number of membrane formulations using plaster, silica gel, sodium silicate, and zeolites were tested in order to improve on the performance of the plaster and silica gel membrane discussed above. None of them demonstrated any significant improvements.

A variety of recipes based on reacting sodium silicate with an acid were tested for making silica gel. Hydrochloric and acetic acids were used. In addition, the gel must be washed to remove the remaining sodium acetate the attempts were not successful at producing useable slabs, because the gel breaks very easily during the drying/polymerization stage. Production of silica gel monoliths is a highly specialized area requiring specialized techniques and skills.

Several formulations were tried to make a membrane from silica gel cemented with sodium silicate. The membranes shrank away from frame after several days and were brittle and crumbled easily (Figure C1).

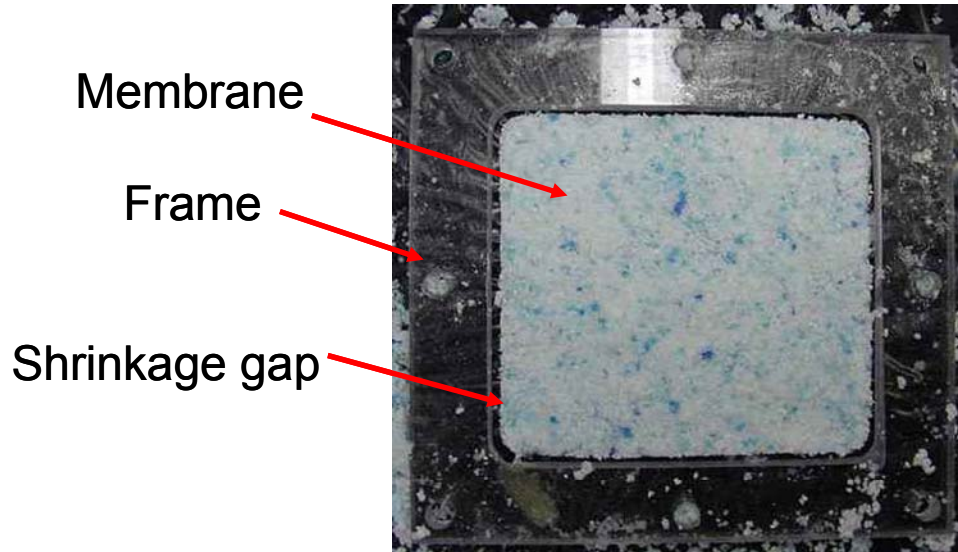


Figure C1: Sodium silicate and silica gel membrane

A membrane was constructed with granular silica gel held between carbon fiber and plastic mesh inside of the plastic frame (Figure C2). This membrane showed a smaller response than the plaster of Paris and silica gel membranes. The gaps between the silica gel particles may have allowed back diffusion of water vapor and possibly the bulk flow of air.

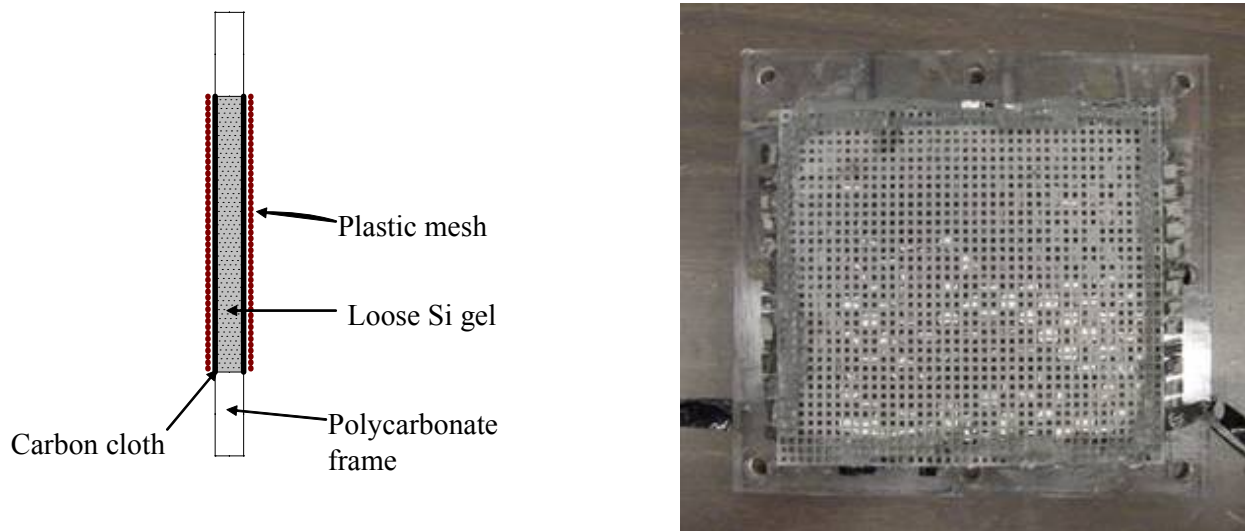


Figure C2: Loose silica gel membrane Right: Schematic side view Left: Photograph of membrane with plastic mesh on top of carbon cloth

Zeolites are porous nano-structured alumino-silicates that are used as desiccants and adsorbents (molecular sieves). Because alumina acts as a base and has an opposite zeta potential to silica it should have the same electroosmotic flow direction as Plaster or Paris. Membranes formulated from zeolite and plaster mix demonstrated flow rates similar to that of the silica gel and plaster membranes.

Membranes fabricated from an agar binder with silica gel granules shrunk away from the frame while drying, but remained flexible (Figure C3). The membrane was glued into the frame with silicone caulk for testing. The membrane did not demonstrate changes in humidity with application of voltage. The agar may act to electrically insulate the silica gel granules from each other, thus reducing the overall membrane conductivity.



Figure C3: Agar- silica gel composite membrane

A plain plaster membrane with embedded stainless steel electrodes was fabricated. The plaster was sanded back to expose the electrodes. This reduced the area covered by the electrode and was intended to reduce the diffusion resistance created by the carbon fiber. However, the performance was similar to that of the plaster and silica gel membrane.